11-30-2003

Modeling Corrosion in Oxygen Controlled LBE Systems with Coupling of Chemical Kinetics and Hydrodynamics-Task V: Fourth Quarterly Report 09/01/2003-11/30/2003

Samir Moujaes
University of Nevada, Las Vegas, samir@me.unlv.edu

Yitung Chen
University of Nevada, Las Vegas, yitung.chen@unlv.edu

Modeling Corrosion in Oxygen Controlled LBE Systems with Coupling of Chemical Kinetics and Hydrodynamics-Task V

Fourth Quarterly Report
09/01/2003-11/30/2003
UNLV-TRP University Participation Program

Principal Investigator: Samir Moujaes
Co-Principal Investigator: Yitung Chen

Purpose and Problem Statement

The Lead-Bismuth eutectic (LBE) has been determined from previous experimental studies by the Russians and the European scientific community to be a potential material that can be used as a spallation target and coolant for the TRP proposed application. Properly controlling the oxygen content in LBE can drastically reduce the LBE corrosion to structural steels. However, existing knowledge of material corrosion performance was obtained from point-wise testing with only very sparse experimental data. Scientists have noticed that the concentration of oxygen dissolved in the liquid alloy could control the corrosion rate of steels exposed to Pb or Pb-Bi. At high oxygen concentration, an oxide layer could be formed on the steel surface (lead oxides are less stable than iron oxide), which protects it from corrosion. At low oxygen concentration, there is no oxidation and corrosion occurs by dissolution of the steel components in the liquid metal. The surface of the oxide layer in contact with the bulk flow of liquid metal may also be eroded under a high fluid velocity. Then the surface of the metal will no longer be protected because a porous oxide layer will be formed.

The first subtask of this project involves using a CFD code (3-D simulation) such as STAR-CD to obtain averaged values of stream wise velocity, temperature, oxygen and corrosion product concentrations at a location deemed close to the walls of the LBE loop at more than one axial location along it. The oxygen and corrosion product inside the test loop will be simulated to participate in chemical reactions with the eutectic fluid as it diffuses through towards the walls. Details of the geometry of these loops will be obtained from scientists at LANL. These values will act as a set of starting boundary conditions to the second task.

The second subtask and the more important objective of this project is to use the information supplied by the first task as boundary conditions for the kinetic modeling of the corrosion process at the internal walls of the test loop. The outcome of the modeling will be fed back to the first subtask, and the steady state corrosion/precipitation in an oxygen controlled LBE system will be investigated through iterations. The information is hoped to shed some light on the likely locations for corrosion and precipitation along the axial length of parts of the test loop.

Personnel

Principal Investigator:

- Dr. Samir Moujaes (Mechanical Engineering)

Co-Principal Investigator:

- Dr. Yitung Chen (Mechanical Engineering)

Students:

- Mr. Kanthi Kiran Dasika, M.S. Graduate Student, (Mechanical Engineering)
- Mr. Narain Armbya, M.S. Graduate Student, (Mechanical Engineering)

National Laboratory Collaborator:

- Dr. Ning Li, Project Leader, Lead-Bismuth Material Test Loop, LANL
- Dr. Jinsuo Zhang, Post Doctoral Candidate, LANL

Adminsitrative Issues:

Some problems arose in continuing our progress due to the fact that one of the solvers provided in STAR-CD that was used for our solutions was not working correctly in the latest version of the code that we received. This delayed our work while we awaited to receive an updated version of that code.

Technical progress:

The technical progress for this quarterly was very intense. One of our students Mr. Chao Wu has finished his thesis on this project and defended his thesis at the end of July, 03. He completed his runs on simulating a 2-D sudden expansion geometry with certain imposed concentration values on the walls downstream from the expansion. This work is in preparation for the 3-D sudden expansion which will be started in Phase III of our project. Mr. Kanthi Dasika will also be finishing shortly and he has had several results to report in this quarter. His task was to perform some grid independency tests on laminar and turbulent flows in different geometries and perform several parametric runs of variations of Re, Sc, oxygen concentration and other important quantities that affect the magnitude of corrosion/precipitation fluxes in a 3-D lead-bismuth flow loop. Mr. Narain Armbya has joined us recently and is working on the 3-D sudden expansion flow models amongst other to broaden our base of information.

Introduction:

Liquid lead-bismuth eutectic is considered as a prototype target and coolant for the Transmutation Research Project (TRP). It is an alloy of 45% lead and 55% bismuth with the melting temperature of 123.5^{o}C and boiling temperature of 1670^{o}C. Using liquid lead-bismuth eutectic (LBE) as coolant in nuclear systems has been studied for more than 50 years. LBE has many unique nuclear, thermo physical and chemical attributes that are attractive for nuclear coolant applications. This liquid's relatively low melting point and high boiling point in addition to good heat transfer properties make it a very good

candidate for coolant. In addition, lead and bismuth can produce copious spallation neutrons when bombarded with energetic protons. This makes LBE one of the top candidates for a high-power spallation target in an accelerator-driven transmutation of waste system. Besides, the use of heavy liquid metal like LBE as a coolant for fast reactors offers several safety and economic advantages. These arise from the following basic material characteristics: chemical inertness with air and water, high atomic number, high boiling temperature and low vapor pressure at operating temperatures. Specifically, heavy-metal coolants do not react energetically with air and water; therefore, coolant fires are not possible and an intermediate heat transport loop is unnecessary. Also, the hard neutron spectrum achievable with these coolants enables the design of cores with minimal neutronic reactivity swing, small control requirements and long neutronic life time. The significantly lower reactivity associated with hypothetical voiding of the coolant, as compared to sodium, makes it possible to design lead or lead-bismuth-cooled cores with a negative coolant void coefficient, there by eliminating the possibility of severe accidents from consideration. Finally, lead or lead-bismuth coolants provide better shielding against gamma-rays and energetic neutrons, so that less shielding structures are needed. Liquid spallation source also eliminates some of the structural damage problems associated with the targets. Combining the target and coolant roles in one material allows for a simple target design.

One of the critical obstacles to the wide use of LBE as a nuclear coolant, though, is corrosion. The corrosion processes need to be controlled and reduced or they lead to severe safety problems. Unprotected steel undergoes severe attack by liquid lead and lead-bismuth alloy by dissolution of its components in the liquid metal. During the last years, not much was known about possibilities to improve the compatibility of steel with liquid Pb and Pb/Bi. Some compatibility tests with ferritic steels were reported which revealed corrosion attack can be minimized if an oxide layer exists on the steel surface. Scientists at IPPE, Obninsk, Russia, discovered that if an oxide film is allowed to form on the steel surface it prevents corrosion. This protective film consists mostly of steel components' oxides and it is based on Fe_3O_4. Formation and longevity of this protective film depends on oxygen concentration on the liquid metal. In order to use liquid lead-bismuth in AAA facility, we need to know how to control corrosion of structural materials.

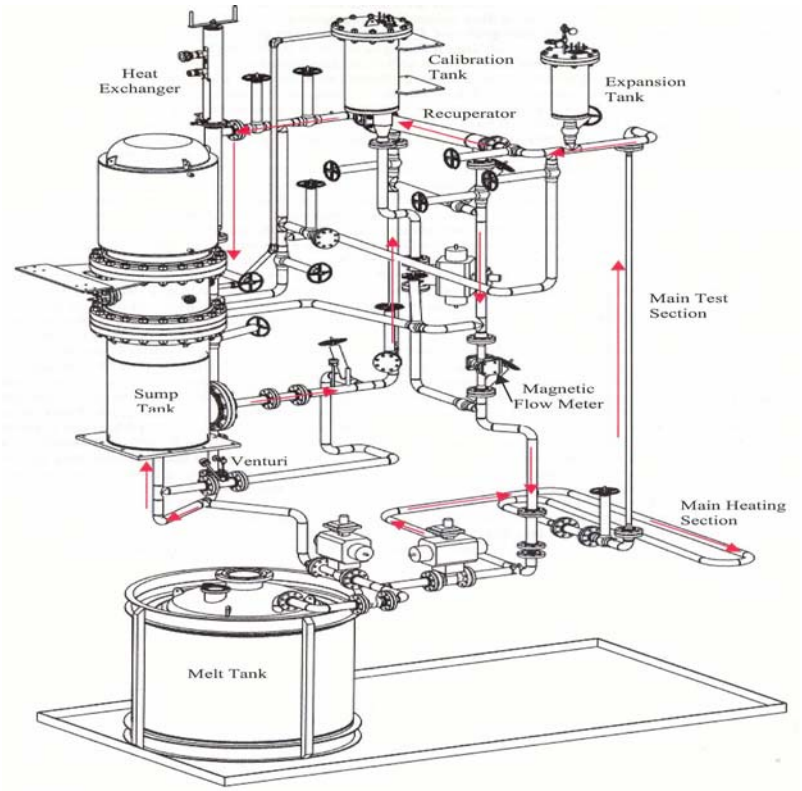

Figure – 1: Materials Test Loop

The active oxygen control technique exploits the fact that lead and bismuth are chemically less active than the major components of steels, such as Fe, Ni, and Cr. By carefully controlling the oxygen concentration in LBE, it is possible to maintain an iron and chrome oxide based film on the surfaces of structural steels, while keeping lead and bismuth from excessive oxidation that can lead to precipitation contamination. The oxide film, especially the compact portion rich in Cr, effectively separates the substrates from LBE. Once this oxide film is formed on the structure surface, the direct dissolution of structural materials becomes negligible because the diffusion rates of the alloying components are very small in the oxides. In this circumstance, the only effective means of transferring structural materials into LBE is through the reduction of the oxide film at the interface of the film and LBE. The Los Alamos National Laboratory's Accelerator-driven Transmutation of Waste (ATW) applications and the Department of Energy's TRP program have invested in developing LBE technology from spallation target and nuclear coolant applications since 1997. A Materials Test Loop (MTL) has been set up in Los Alamos. The MTL is a facility designed to test the safe operation of a medium-size, forced circulation LBE system with representative thermal hydraulic conditions (as spallation target and/or transmutation blanket systems), to perform corrosion tests, and to develop candidate materials with oxygen control (and related probes and control systems). Figure-1 shows the skeleton representation of the MTL.

It has been well known that fluid flow influences corrosion in many ways, including the increase of the diffusion of reactant species and the transport of potentially protective corrosion product forming ions away from surface. In the mass transfer controlled

regime, the corrosion rate is determined by the mass transfer coefficient and the gradient between the corrosion product concentration at the solid-liquid interface and the concentration in the bulk flow. Corrosion rate is typically a function of local temperature and flow velocity. However, corrosion and precipitation rates and distributions can depend strongly on the global temperature distribution, limiting the applicability of many corrosion models.

The present study involves the estimation of corrosion in the liquid metal, by imposing an analytically developed concentration expression on the wall surfaces and thus benchmarking the CFD tool and performing a series of parametric studies on the loop model. The concentration and temperature diffusions due to different flow regimes have been studied. Regions of maximal corrosion and precipitation have been deduced from the simulations and the results have been compared with the analytical models. STAR-CD has been chosen as the CFD code for this purpose.

Numerical Simulation Technique:

The STAR-CD computer simulation code was chosen for the purpose of performing the Computational Fluid Dynamics (CFD) calculations for this project. STAR-CD is a commercially available code that is offered by ADAPCO Co. out of New York State. The code is a transient multidimensional simulator for Thermal hydraulics and chemical reactions occurring in the fluid flow itself.

STAR-CD is a general-purpose code that solves numerically a set of differential equations that describe the following conservation laws: mass conservation, momentum, energy and chemical species. The following equations are solved by this code:

Continuity Equation:

$$u_{i,i} = 0 \tag{1}$$

Momentum Equation:

$$\rho_0[\frac{\partial u_i}{\partial t}+u_i u_{i,j}] = - P_{,i} +[\mu(u_{i,j}+u_{j,i})]_{,j} \tag{2}$$

Energy Equation:

$$\rho_o C_p(\frac{\partial T}{\partial t} +u_i T_{,i})=(K*T_{,i})_{,i}+\mu\Phi \tag{3}$$

Species Transport:

$$\rho(\frac{\partial C_n}{\partial t} + u_i C_{n,i}) = (\rho\alpha_n C_{n,i}) + q_{c_n} + R_n \tag{4}$$

Due to the Re number estimate for flow in a LBE loop a turbulent flow model should be used as a constitutive model for the momentum transport. It was decided that a k-ε model is to be used to account for that behavior. The model consists of adding two more non-linear (transport equations) partial differential equations to each unknown nodal location. The k denoted the turbulent kinetic energy $\overline{u_i u_i}$ and the ε is the viscous dissipation rate of the turbulent kinetic energy $\upsilon\overline{u_{i,j}u_{i,j}}$. The resulting equations are:

k – transport equation:

$$\rho_o\left(\frac{\partial k}{\partial t} + u_i u_{i,j}\right) = \left(\mu_o + \frac{\mu_t}{\sigma_k} k_{,j}\right)_{,j} + \mu_t \Phi + \mu_t g_i \left(\frac{\beta_T}{\sigma_t} T_{,j}\right) - \rho_o \varepsilon \qquad (5)$$

ε – transport equation:

$$\rho_o\left(\frac{\partial \varepsilon}{\partial t} + u_j \varepsilon_j\right) = \left(\mu_o + \frac{\mu_t}{\sigma_k}\right)_{,j} + c_1 \frac{\varepsilon}{k} \mu_t \Phi + c_1 (1 - c_3) \frac{\varepsilon}{k} g_i - \rho_o c_2 \frac{\varepsilon^2}{k} \qquad (6)$$

Overall Corrosion Modeling:

Benchmark Study:

This section sheds light on the velocity, temperature and concentration profiles obtained by assuming the MTL as a rectangular loop model. The results are shown for the flow in both the laminar and turbulent regimes, which is followed by the comparison of the analytical and simulation results. Finally, the results are shown to be grid independent.

Laminar Flow:

The model has been run with the boundary conditions specified in the second chapter with the inlet velocity of 0.004m/s resulting in a Reynolds number of 2000. Figure 2 shows the velocity profile at a diametrical section cut along the loop length. The velocity along the whole loop length is shown in the figure. The velocity profiles look reasonable as the parabolic profiles have been seen in the straight run of the loop. There is a slight eccentricity in the center of the parabola, which can be explained as due to the presence of the elbows which causes the disturbance in the flow.

The velocity at the elbow section is shown separately in the Figure 3. The elbow section shown in the figure is in the region of the main test section of the LBE. The figure shows the diametrically cut away section at the elbow.

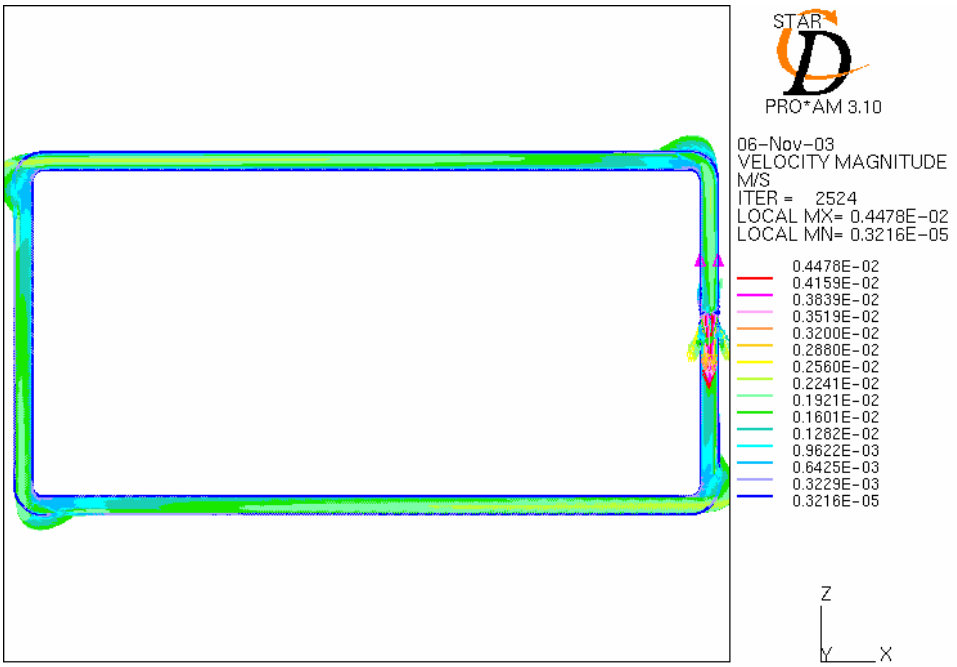

Figure – 2: Velocity Profile in the Overall Loop Length for a Laminar Rectangular Loop Model

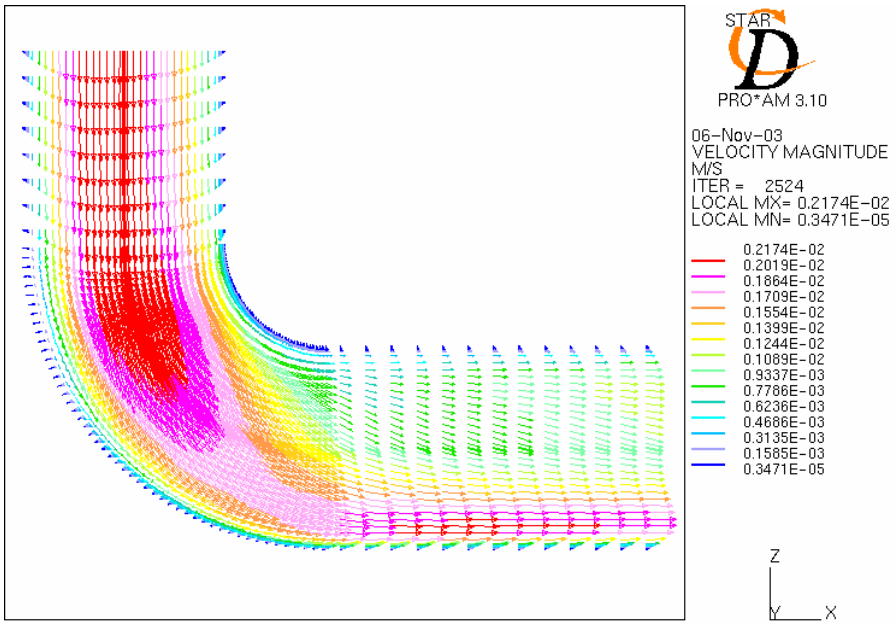

Figure–3: Velocity Profile at an Elbow Section of the Laminar Rectangular Loop Model

Figure 4 shows the temperature profiles along the whole length of the loop of the MTL. The diffusivity of the wall temperature into the bulk is clearly visualized in the figure and is more prominent in the transverse direction than in the lateral direction due to low velocity of the flow.

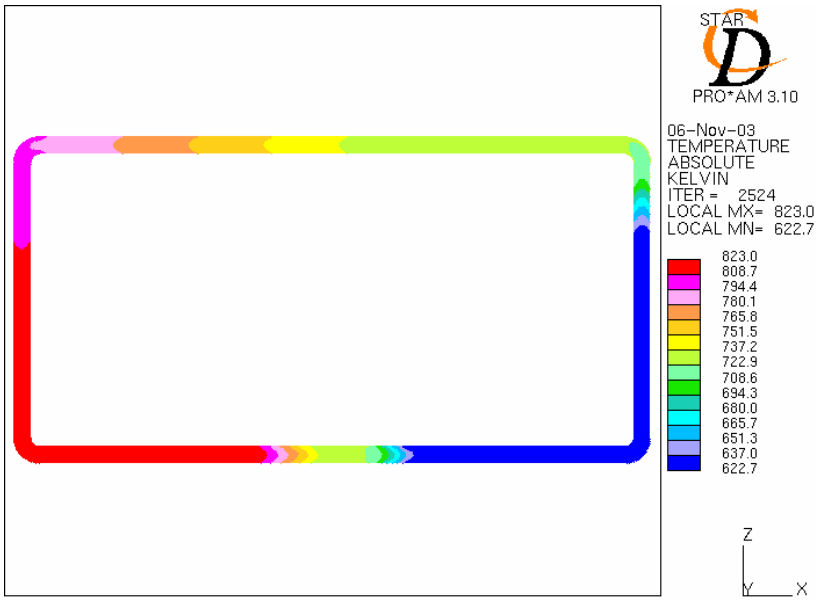

Figure – 4: Temperature Profile in the Overall Loop Length for a Laminar Rectangular Loop Model

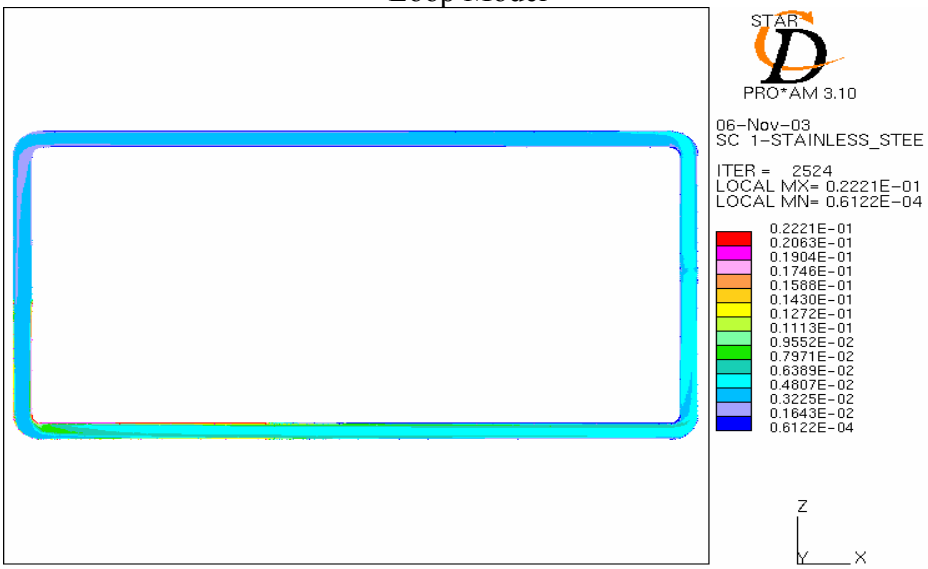

Figure – 5: Concentration Profile in the Overall Loop Length for a Laminar Rectangular Loop Model

A similar argument applies for the wall concentration diffusion, which is shown in the figures 5 and 6 at the same two locations described above. The figures shown are the section views cut along the diameter of the loop. The wall temperature and concentration are imposed according to figure 2.

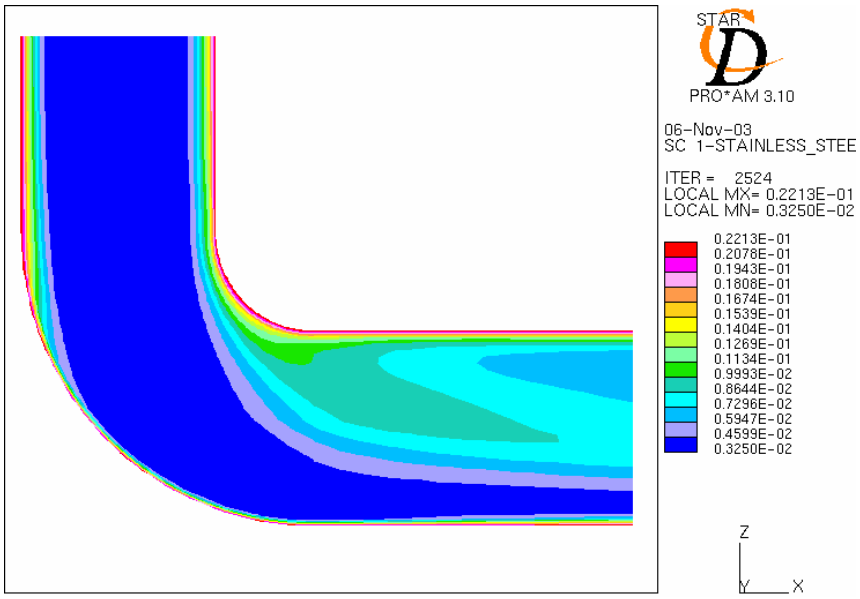

Figure – 6: Concentration Profile at an elbow section for a Laminar Rectangular Loop Model

It can be inferred from the above figures that the profiles of the various thermal hydraulic profiles and the mass transfer profiles show the trends as expected. The results still need to be compared with the analytical results to strengthen the above statement. The parameter of comparison remains the corrosion/precipitation rate along the loop length. The plot obtained for the same parameter using the simulation model is shown in Figure 7. A keen observation of the two figures helps deduce the fact that the trends from both the analytical and simulated models look very similar excepting for a few sections, the reasons of which has been elaborated in the following discussion. The maximum and minimum corrosion rate values do not coincide due to the difference in the flow regimes for the analytical and simulation models.

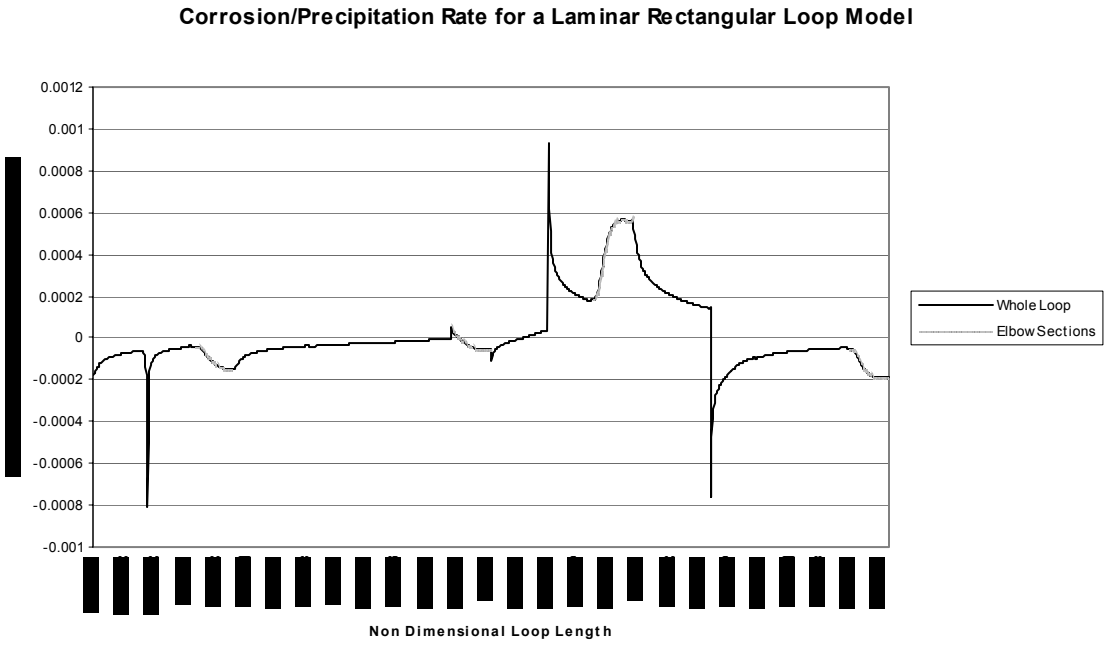

Figure – 7: Corrosion/Precipitation rate for a laminar closed rectangular loop model assumption of the Materials Test Loop

In Figure 7, the graph has two different line patterns. The solid line corresponds to the corrosion/precipitation rate along the whole length of the loop, where as the dotted lines correspond to the elbow sections of the loop. These sections have been highlighted to illustrate the effect of the elbow sections on the corrosion rate. It is a well-known fact that the secondary flows act in an elbow section and this causes the disruption in the diffusivity of the temperature and concentration. It should be mentioned here that the concentration gradient has been calculated by averaging at four different points that are located on the inside, outside and the two sides on the circumference of the circular cross section along the loop length. This gives a more precise value than choosing a single point for calculating the corrosion rate. One other point of variation is at the section slightly downstream from the zero length. A steep dip in the corrosion rate can be seen at this point. This dip is caused due to the momentum source term incorporated to replicate the pump.

For presenting a detailed insight into the effect of velocity variations on the diffusion of the mass transfer from the wall into the bulk flow at the elbow sections, the velocities and concentrations along the four points mentioned above at one elbow section have been plotted separately. Also extracted are the velocity and concentration contours at three different cut away sections of the elbow normal to the flow.

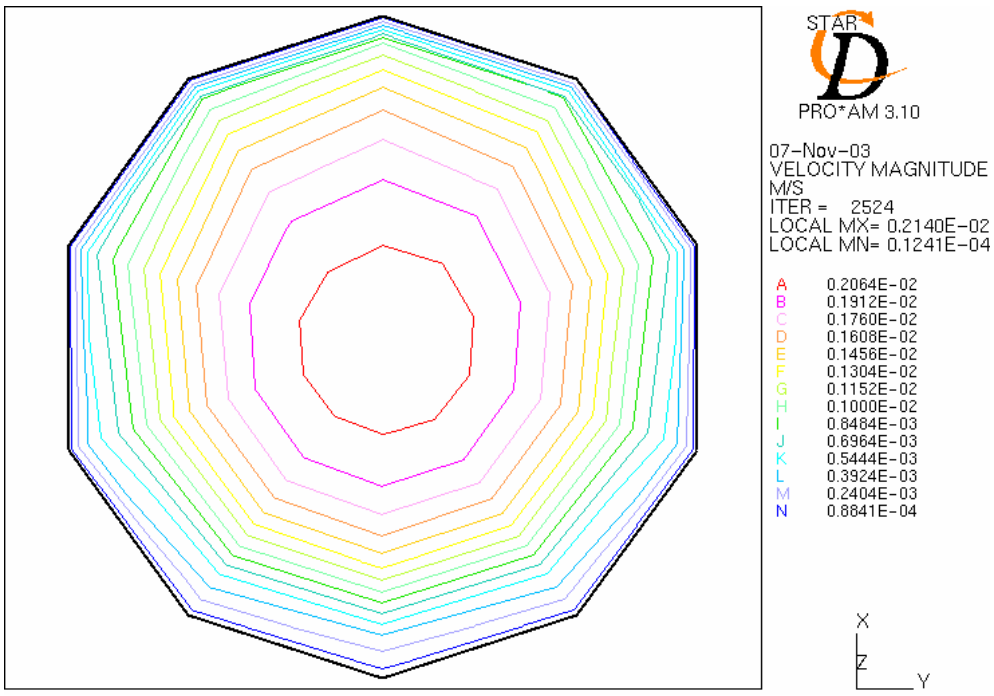

Figure – 8: Velocity contour at the first elbow cut away section normal to the flow

Figures 8 and 9 show the velocity and concentration profile at a section sliced normal to the flow in the elbow in the region of main test section. This section is located geometrically at a few cells downstream after the elbow section begins. The top edge in the figure corresponds to the inside edge of the elbow and the bottom edge in the figure corresponds to the outer edge of the elbow section.

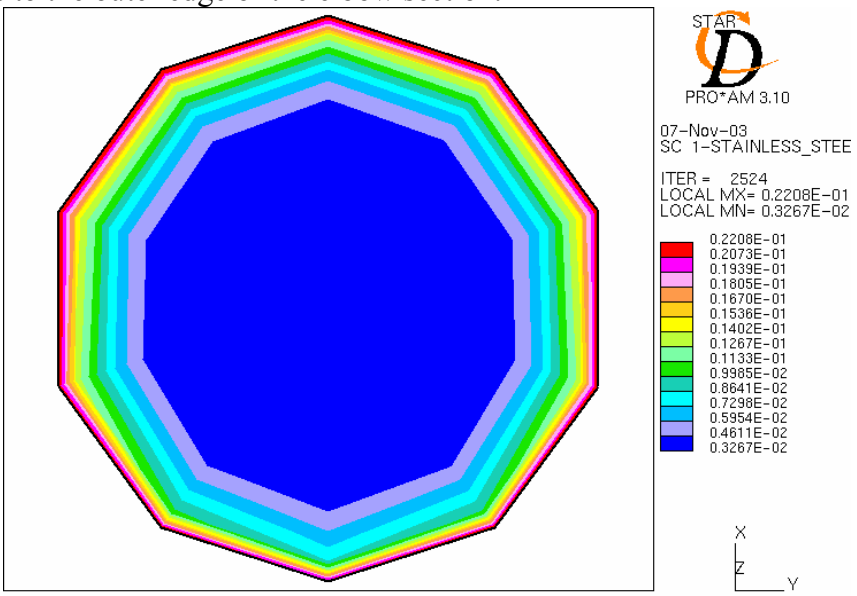

Figure – 9: Concentration profile at the first elbow cut away section normal to the flow

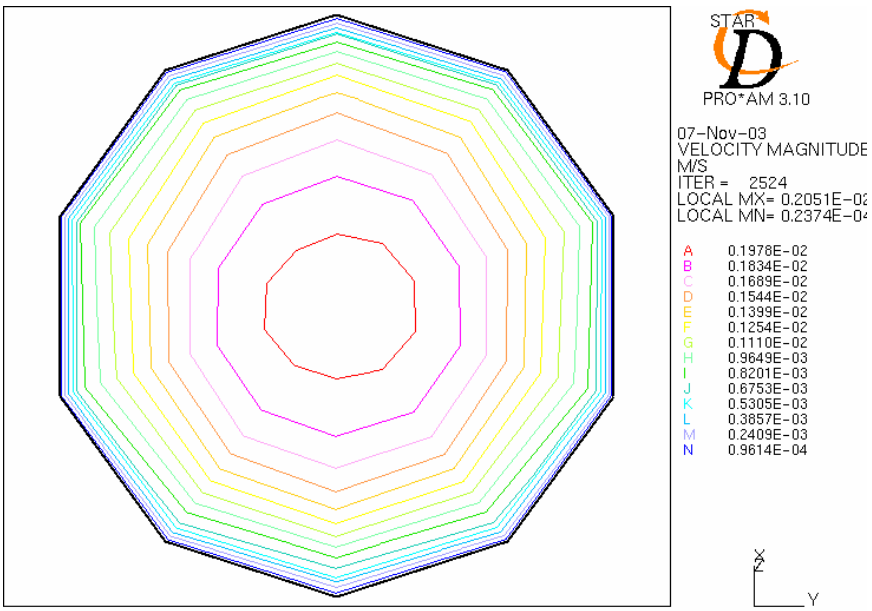

Figure – 10: Velocity contour at the second elbow cut away section normal to the flow

Figures 10 through 13 show the velocity and concentration profiles at the section slices along the elbow further downstream. Figures 10 and 11 are geometrically located at the middle of the elbow and the figures 12 and 13 are at the end of the elbow section. As anticipated, the inside edge of the sections of the elbow have higher dissemination rate than the outside edge.

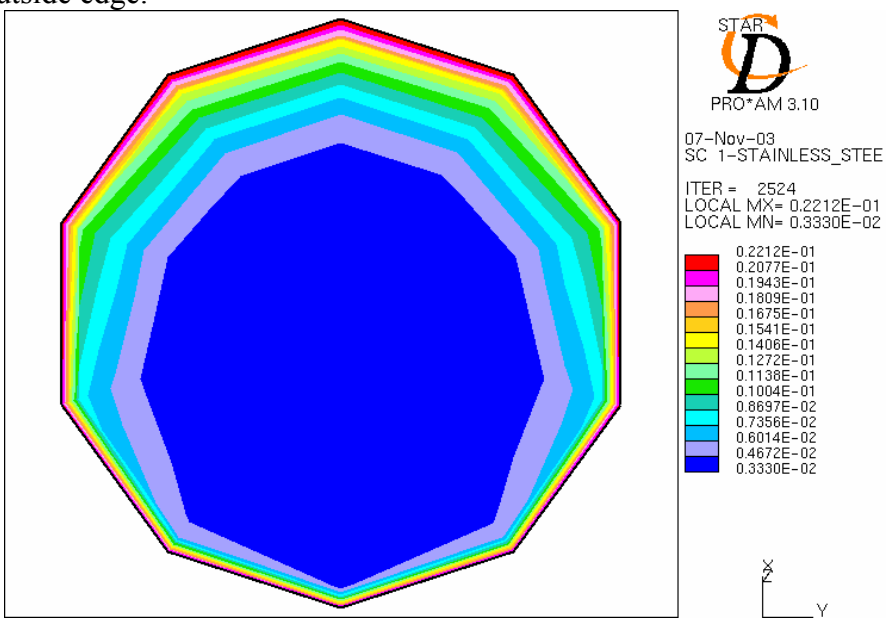

Figure–11: Concentration profile at the second elbow cut away section normal to the flow

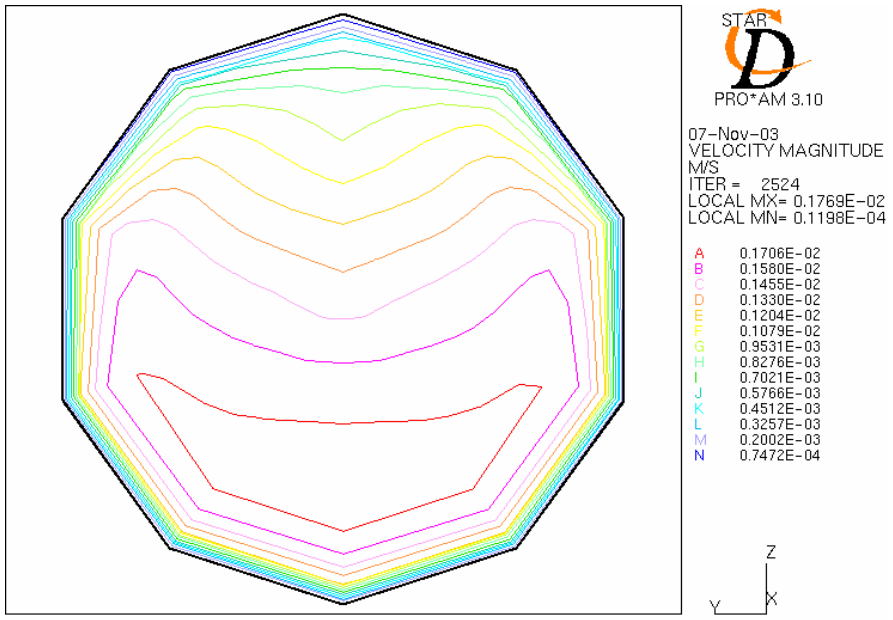

Figure – 12: Velocity contour at the third elbow cut away section normal to the flow

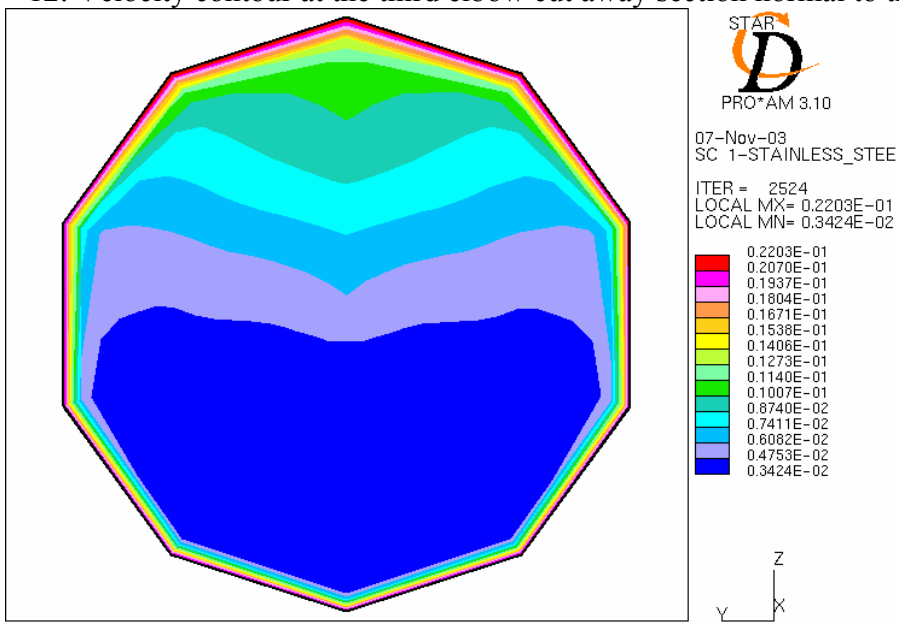

Figure – 13: Concentration profile at the third elbow cut away section normal to the flow

The figures 14 and 15 depict the velocities and concentrations plotted at the three edges of an elbow, namely inside edge, outside edge, and the edge on the side along the flow direction. These figures make obvious the fact that the increment of the velocities result in decrease in the rate of corrosion.

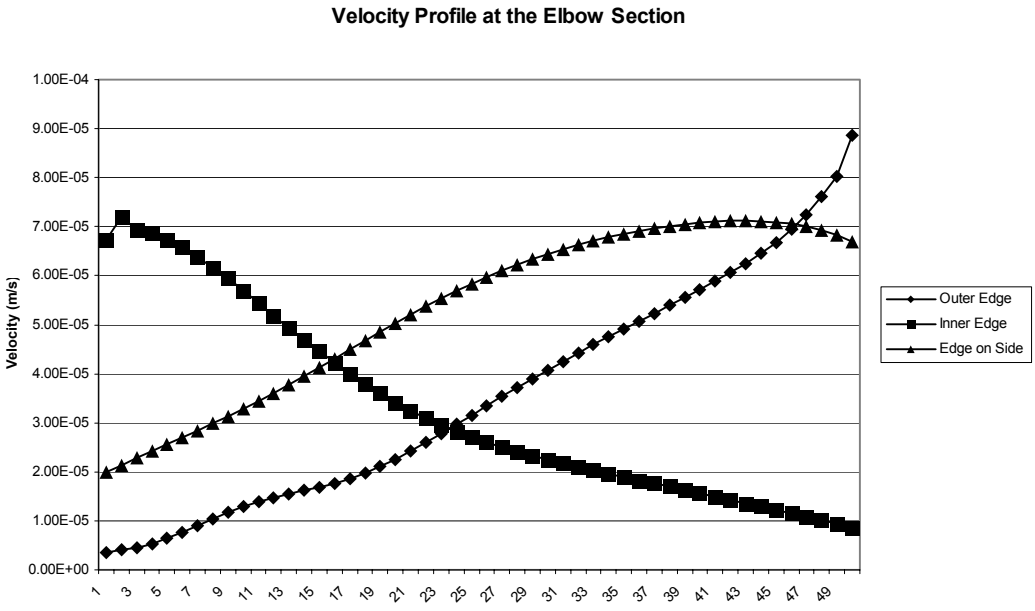

Figure – 14: Velocity profile on the edges of the elbow section

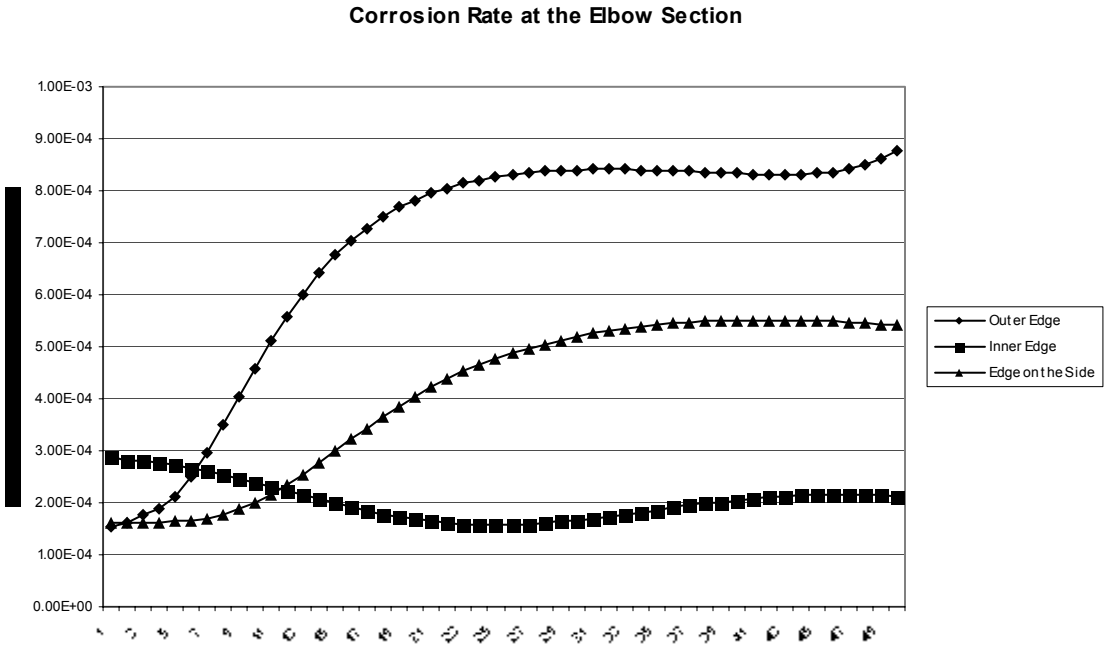

Figure – 15: Rate of corrosion change on the edges of an elbow section

The detailed deliberation of the effect of the secondary flows at the elbow sections and the consequent variation in the diffusivity justifies the peculiar trend of the corrosion/precipitation rate at the elbow sections in figure 7. Hence, it could be concluded that the results of the simulation are fairly accurate. But before any further analysis could be carried out, it should be made sure that the results are grid independent. The following confabulation outlines the grid independency test.

The process of grid independency check is similar to the method adopted for the grid independency test of the open straight pipe model. Three different grid structures outlined in the previous chapter have been used for running the same analysis.

Figure 16 shows the result from the grid independency check. The values on the inside edge, outside edge and the edges on the two sides have been averaged for all the three grid structures and overlaid in the same graph. It can be seen from the figures that the results are grid independent. The 'fine' and 'finer' grid structures stay almost on the top of each other. For this reason, the 'finer' grid structure has been incorporated for the results discussed above and for further analysis.

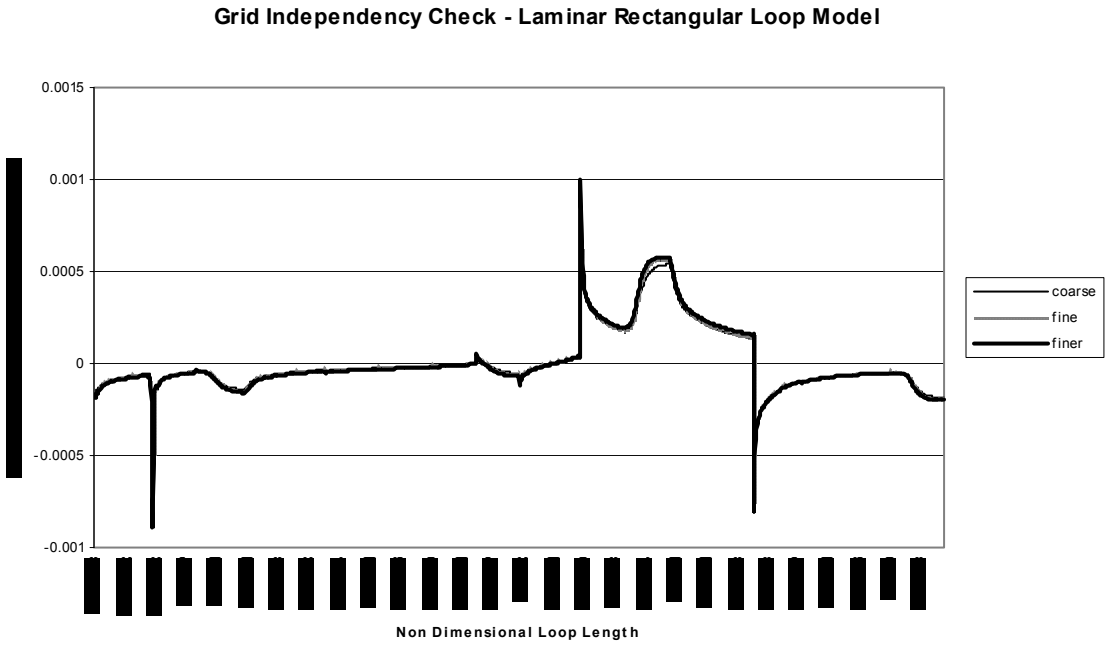

Figure – 16: Grid Independency Check for a Laminar Rectangular Loop Model

Turbulent Flow:

The model has been run for a turbulent flow regime with an inlet velocity of 0.4m/s and a Reynolds number of 200000. Figures 17 and 18 show the velocities at a section cut diametrically over the whole loop length and at an elbow section. The elbow section is physically located at the main test section of the MTL.

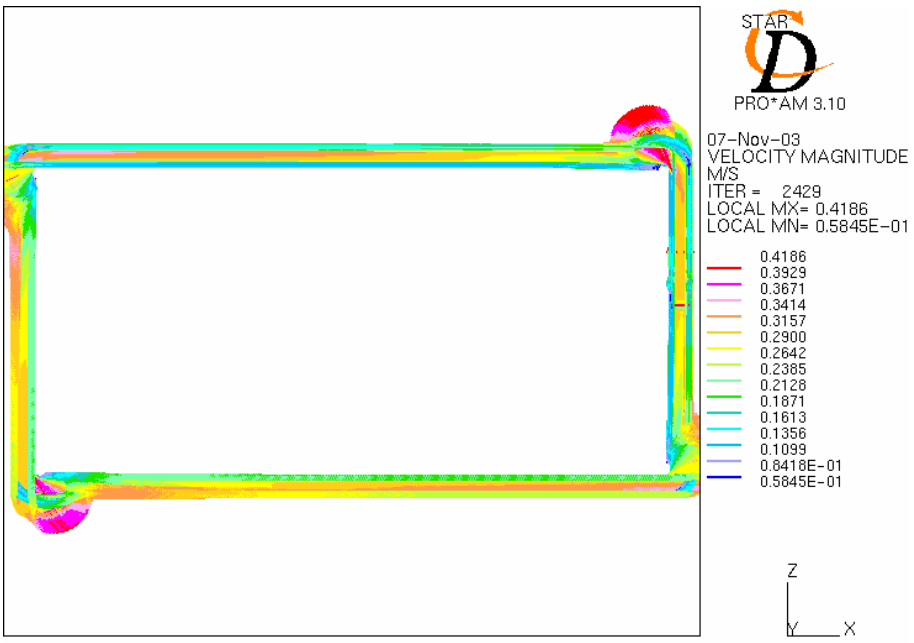

Figure – 17: Velocity profile in the overall loop length for a turbulent rectangular loop Model

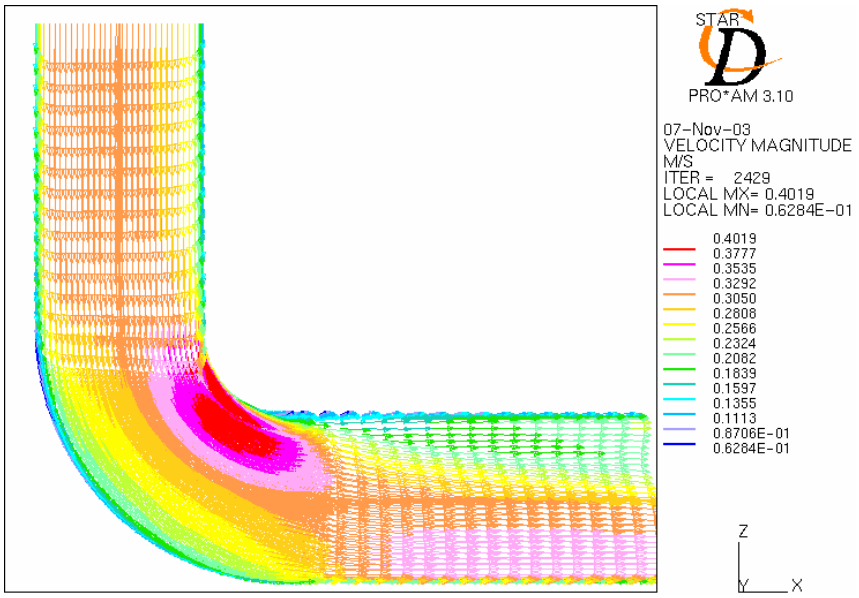

Figure – 18: Velocity profile at an elbow section for a turbulent rectangular loop model

Figure 19 shows the temperature profile at a diametrical section along the loop length. It is noticeable that the temperature diffusion from the wall into the bulk of the fluid is not as significant as it is for the case of a laminar flow. This is essentially due to the more prominent velocities in the former case than the latter case. The higher velocities in the turbulent flow make the diffusion more predominant in the lateral direction than the transverse direction.

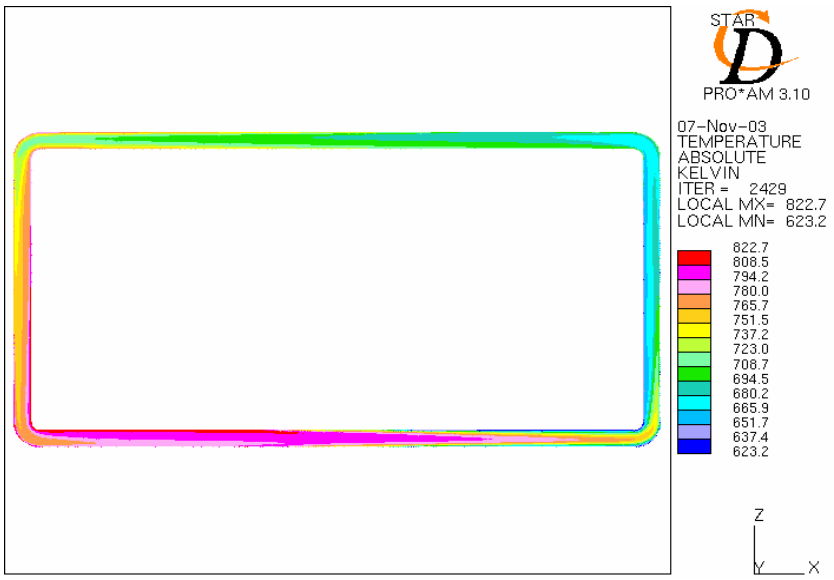

Figure – 19: Temperature profile in the overall loop length for a turbulent rectangular loop Model

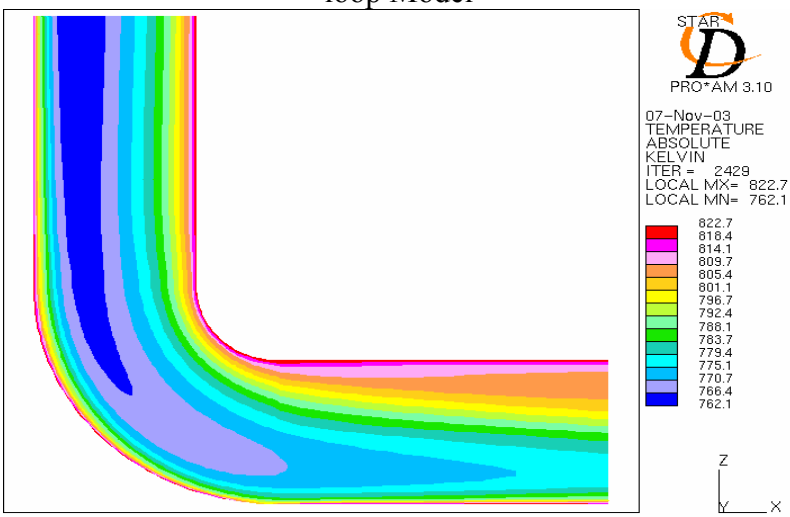

Figure–20: Temperature profile at an elbow section for a turbulent rectangular loop model

Temperature distribution in an elbow cut away section is shown in the figure 20. For the turbulent case too the wall temperature and concentration profiles are imposed according to figure 2.

The concentration profiles at the above two locations are shown in figures 21 and 22. The reasoning of the lower diffusion rate in the transverse direction than the lateral direction applies for the case of corrosion too. This results in a uniform mixing of the concentration in the case of a turbulent flow.

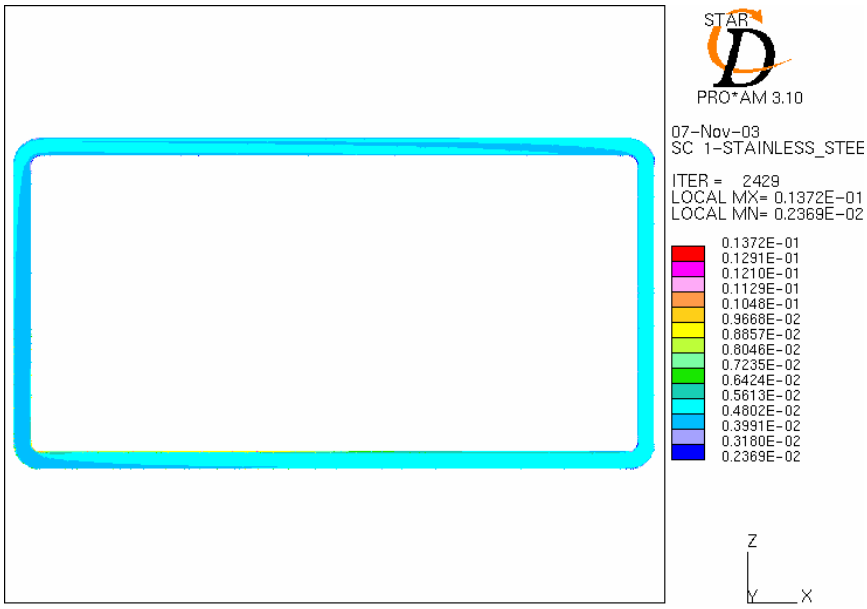

Figure – 21: Concentration profile in the overall loop length for a turbulent rectangular loop Model

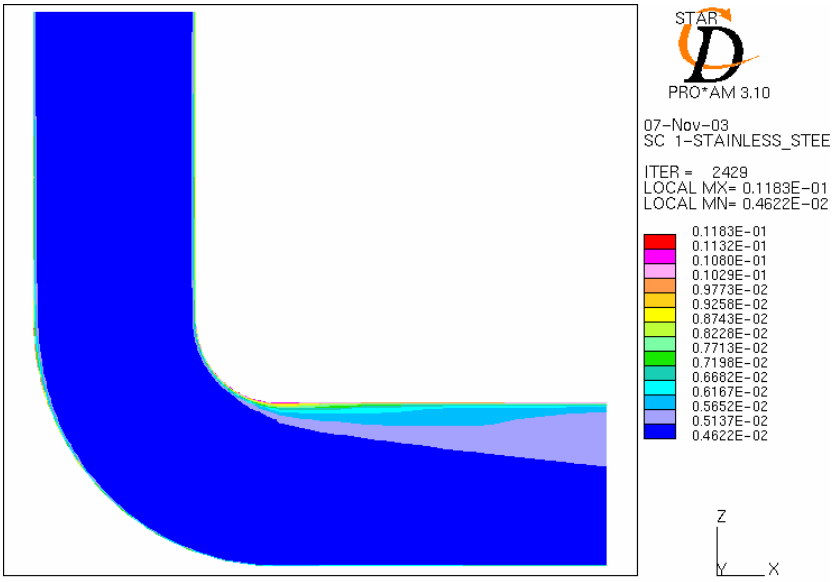

Figure – 22: Concentration profile at an elbow section for a turbulent rectangular loop model

As discussed previously, the next step towards benchmarking is the comparison of the analytical results with the simulation results. Figure 24 shows the corrosion/precipitation rate for the turbulent rectangular loop model assumption of the MTL from the simulation. For this case also, the concentration has been averaged at four different edges of the circular cross section, namely, the inner edge, the outer edge and the edges on the two sides. This has to be compared with the figure 23, which shows the analytical result for a turbulent closed straight loop model assumption. Close observation of these two figures reveals that the curve patterns look alike excepting at a few sections. The amount of corrosion/precipitation rate in cm/yr also coincides closely with the analytical results. The

discrepancies in the trends are distinguishable mainly at the elbow regions and at the region where the momentum source has been applied. The elbow regions have been highlighted in the figure for a better sagacity.

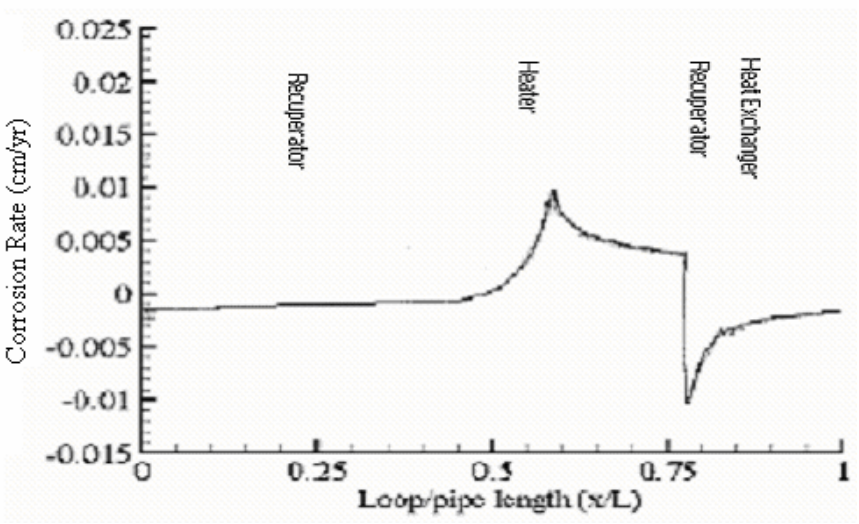

Figure – 23: Corrosion/Precipitation Rate for a Turbulent Closed Straight Loop Model Assumption of the Materials Test Loop

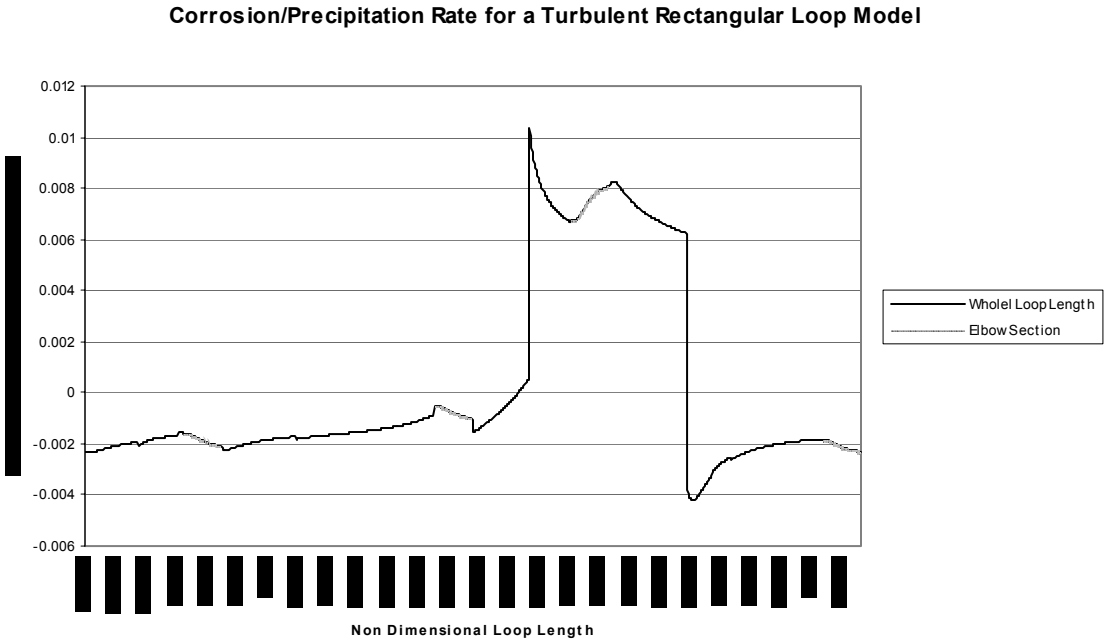

Figure – 24: Corrosion/Precipitation rate for a turbulent closed rectangular loop model assumption of the Materials Test Loop

From the figure 24, it is lucid that there is an increase in the rate of corrosion/precipitation at one elbow region and there is a decrease in the other three regions. The elbow region where there is an increase in the value falls in the corrosion zone and the other regions where there is a decrease in the value falls in the precipitation zone. In other words, both the rate of corrosion and the rate of precipitation increase in their respective zones, which helps deduce the detail that the elbow regions and the secondary flows formed in these regions intensify the effect of corrosion and precipitation in their respective regions.

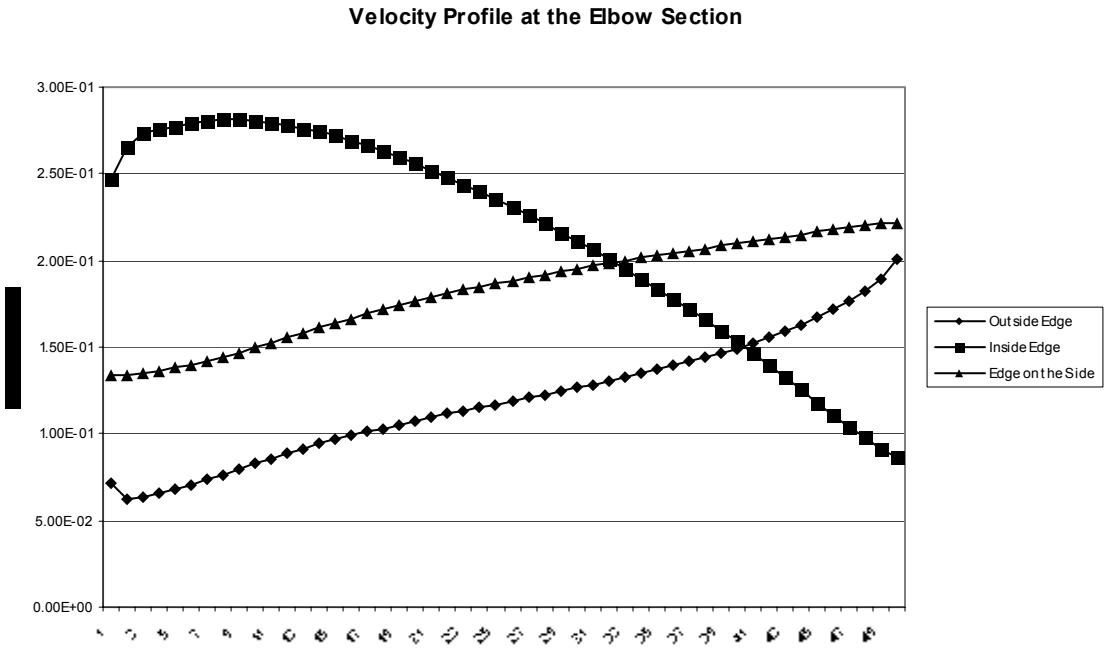

Figure – 25: Velocity profile on the edges of the elbow section

To authenticate the above conclusion a more comprehensive study on one of the elbow regions has been performed. The edges specified above (inner edge, outer edge, edge on the side) have been taken into consideration and the velocity and concentration profiles at these three edges have been plotted. Figure 25 shows the velocity variation in the flow direction in the elbow region at the three different edges pointed out above. At the same locations, the corrosion rates have been plotted in a graph that is shown in figure 26. By comparing these two figures, it can be excogitated that the increase in velocity increases the corrosion rate and the decrease in velocity decreases the corrosion rate. This is true in the case of precipitation rate also, where the increase / decrease in velocity increases / decreases the precipitation rate respectively.

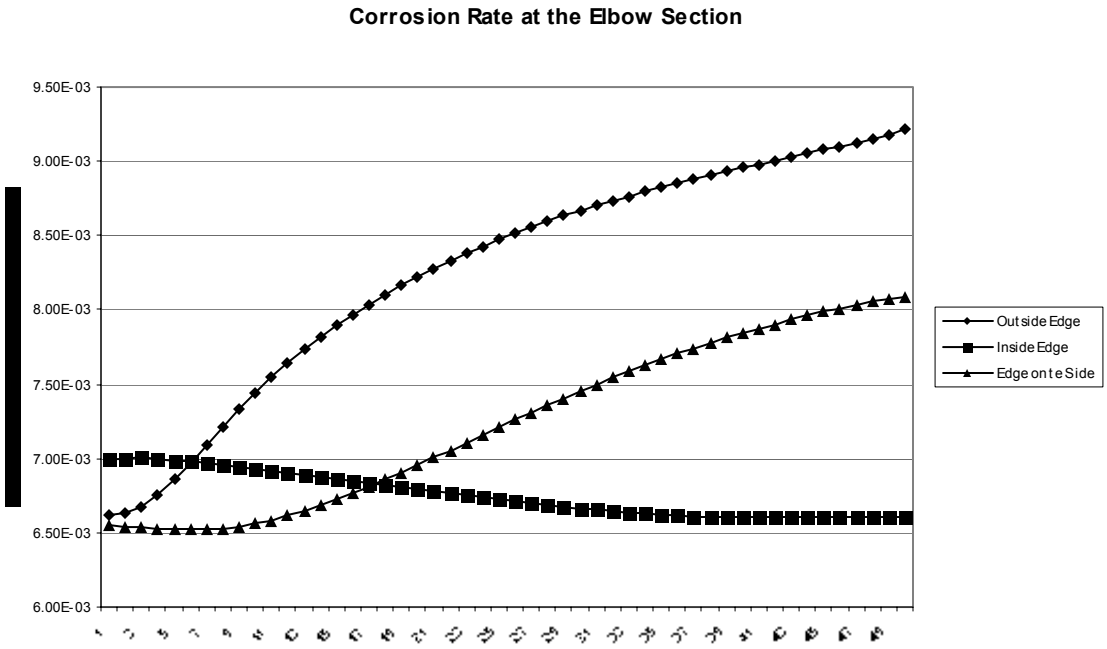

Figure – 26: Corrosion/Precipitation rate on the edges of the elbow section

Further insight into the secondary flows in the elbow section has been provided in the following discussion. Three different cut away sections normal to the flow direction have been shown below. The sections are located at the start, middle and end locations of the elbow present at a section analogous to the main test section of the MTL.

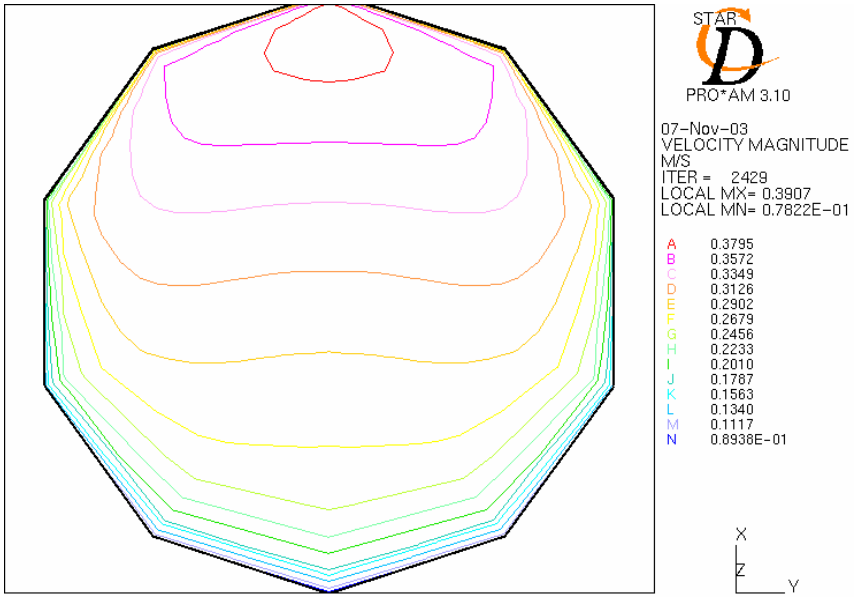

Figure – 27: Velocity contour at the first elbow cut away section normal to the flow

The streamline velocity contours and concentration profiles at these three locations have been presented in the figures 27 through 32. Figures 27 and 28 show the velocity contour

and concentration profile at the starting location of the elbow section. It can be seen that the secondary flows start developing eddies in the region. And the higher concentration zones, as can be seen, correspond to the higher velocity regions, which further invigorate the statement above.

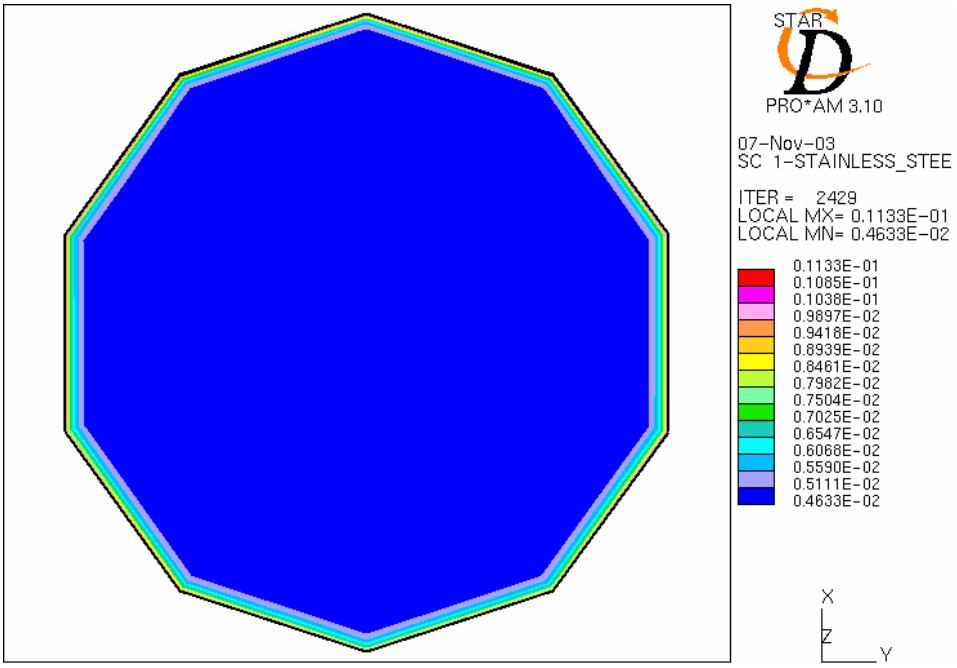

Figure – 28: Concentration profile at the first elbow cut away section normal to the flow

Figures 29 and 30 show the velocity and concentration of the section of the elbow further downstream. The secondary flows develop further and result in higher concentration on the inside edge of the elbow. This section is located at the middle of the elbow.

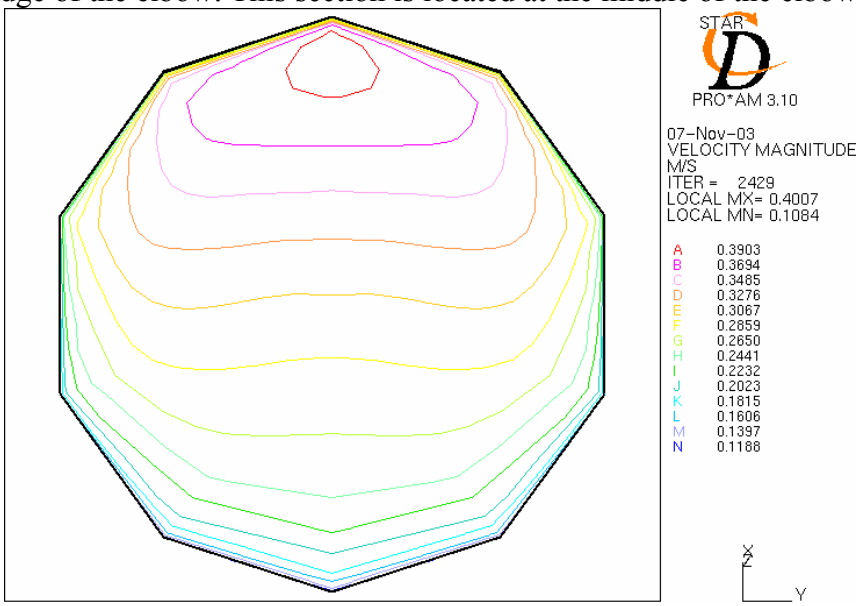

Figure – 29: Velocity contour at the second elbow cut away section normal to the flow

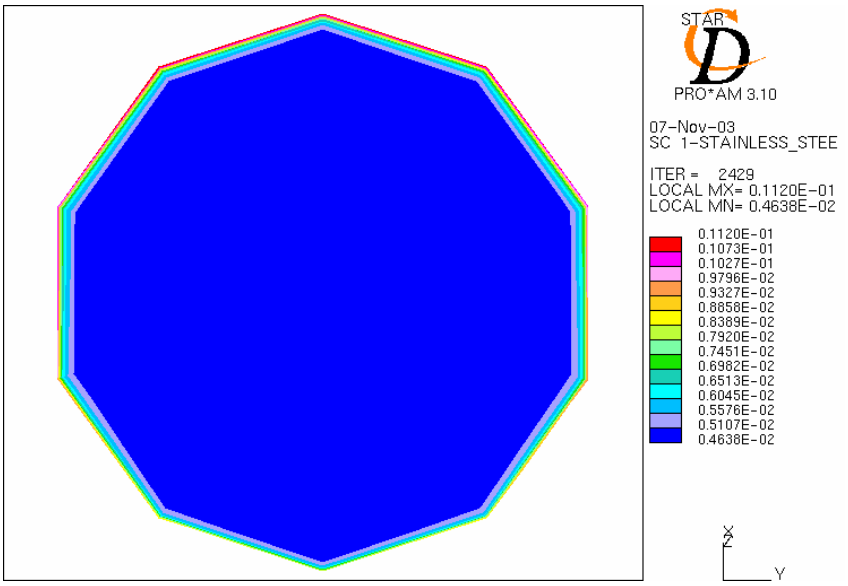

Figure–30: Concentration profile at the second elbow cut away section normal to the flow

Figures 31 and 32 show the velocity and concentration at the end of the elbow section. The higher concentration zone advances more towards the center when compared with the previous two sections of the elbow due to eddies.

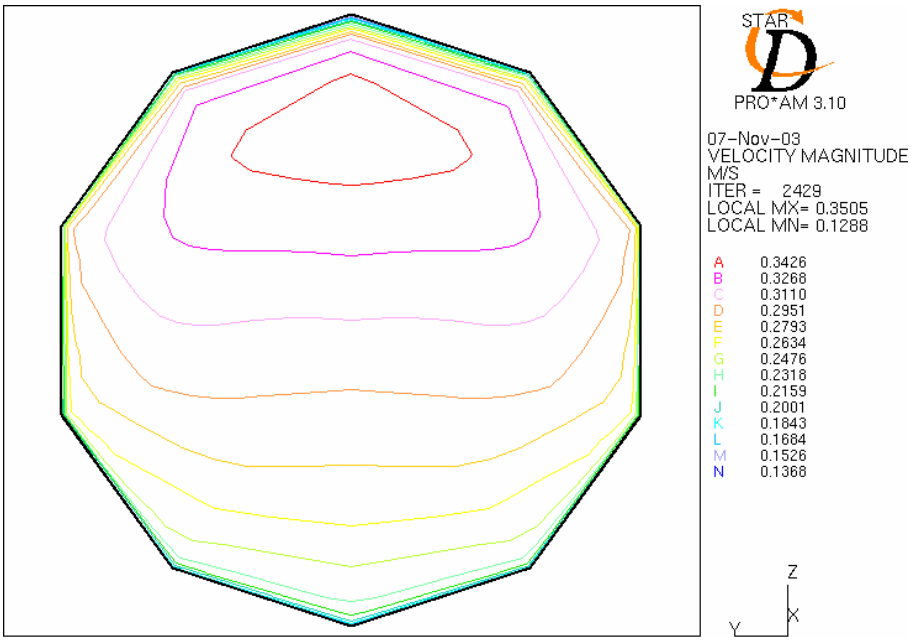

Figure – 31: Velocity contour at the first elbow cut away section normal to the flow

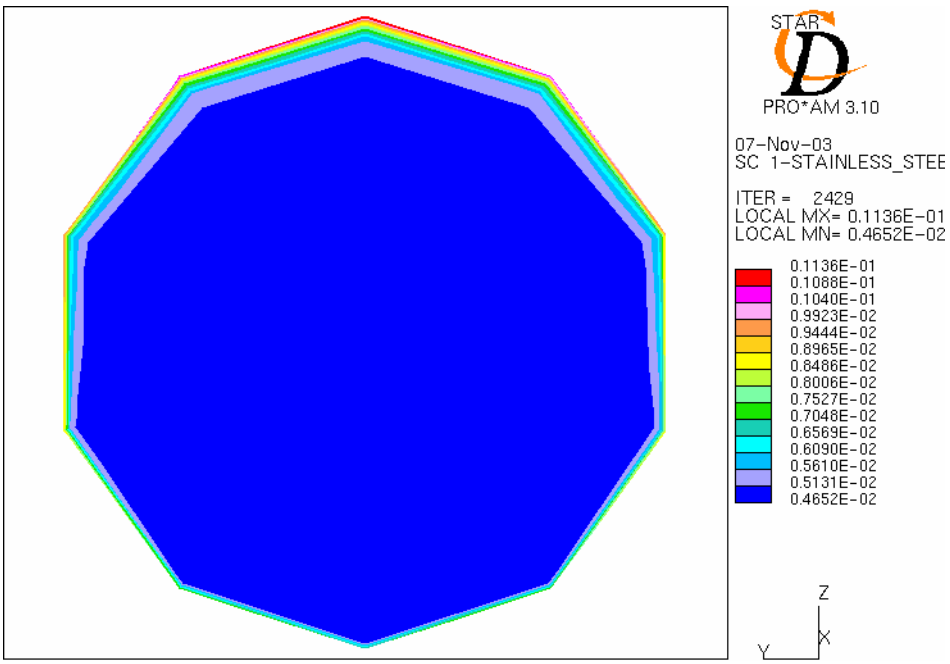

Figure – 32: Concentration profile at the first elbow cut away section normal to the flow

The above deliberation theorizes the active participation of the secondary flows in the corrosion of the MTL and the good tune of the simulation results with the analytical results lays good foundation for the benchmarking process. The final check, though, for the benchmarking process is to check for the dependency of the obtained results on the grid structure. Figure 33 shows the graph depicting the grid independency check. Similar procedure of considering three different grid structures and running the model with the same boundary conditions has been followed. The corrosion/precipitation rate from all the three runs has been compared. It can be seen that the results do not vary by a lot with the change in grid structure. The percentage error in the 'fine' and 'finer' grids seems to be in a better agreement than the 'coarse' grid. Hence it could be concluded that the results from the 'fine' grid structure are independent of mesh distribution.

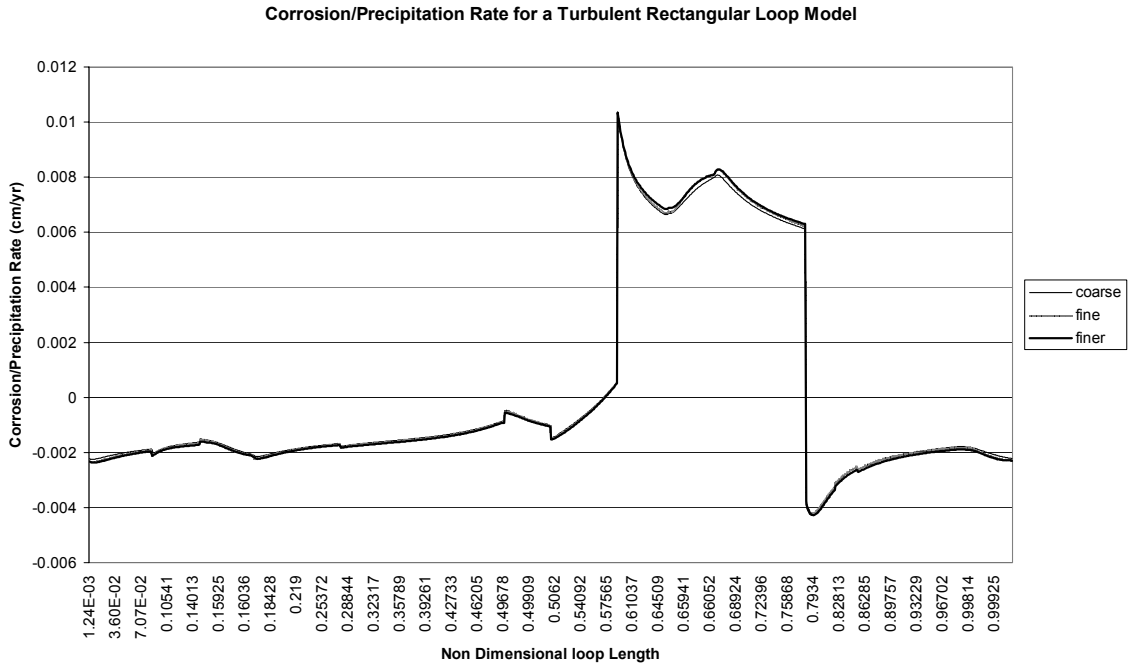

Figure – 33: Grid independency check for a turbulent rectangular loop model

This study helps deduce the fact that the simulation results are in good tune with the analytical results and hence the process of benchmarking the CFD code is successful. The research has then been extended to further analyze the effect of various parameters on the mass diffusion which has been outlined in the following section.

PARAMETRIC STUDY:

A parametric study has been carried out for the rectangular loop model with Reynolds number, Schmidt number, initial oxygen concentration and temperature variation along the loop length as parameters. The studies have been carried out both in the laminar and turbulent regimes. The parametric studies are mainly useful in determining the most critical points in the MTL i.e. the points of maximal or minimal corrosion and helps decide on the most favorable parameters to run the loop with longest possible life. The parametric study cases for each parameter have been analyzed separately in the following discussion.

Reynolds Number:

Reynolds number plays a very vital role in the area of thermal hydraulics. It directly influences the mass diffusion rate in a pipe flow. The mass diffusion rate in turn affects the corrosion or precipitation rate in the MTL. Hence, the behavioral study of the mass diffusion with the variation of velocity makes a very interesting topic for the present case. For this reason, a parametric study of the Reynolds number has been carried out. The studies were limited to the turbulent flow because of the fact that the flow effects on mass

diffusion are more predominant for high Reynolds numbers than for the low Reynolds numbers.

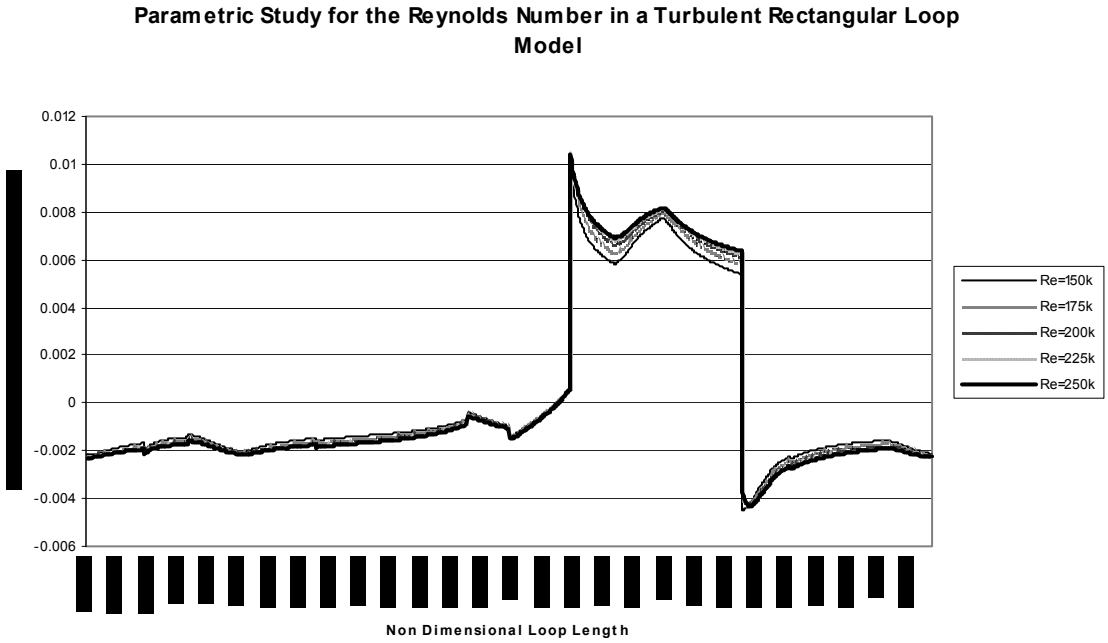

Figure – 34: Parametric Study in Reynolds Number for Turbulent K-ε Flow

The parametric study consisted of flow modeling at five different Reynolds numbers. The range of Reynolds numbers considered were: 150000, 175000, 200000, 225000, and 250000. The simulations were carried out with all the remaining parameters kept at the pre-defined values for the benchmark study. Since the main focus of study is the corrosion/precipitation rate, the results of these rates have been extracted. These results, from all the runs have been plotted against the non-dimensional loop length, as shown in the figure 34.

As can be seen, the concentration flux from all the five runs almost overlap excepting at a few places. The maximal corrosion/precipitation point almost stays the same for all the runs. The only region where the variation is considerable is the region after the point of maximal corrosion and before the point of minimal corrosion. An elbow is present in this region and the region where the elbow is present has the maximum effect on the corrosion/precipitation rate. Apart from that, the effect of the Reynolds number in the given range is negligible on the corrosion/precipitation rate.

Schmidt Number:

The next parameter considered for analysis is the Schmidt number. Schmidt number is the ratio of kinematic viscosity and diffusivity. For the parametric study, the kinematic viscosity has been kept constant and the diffusivity has been varied. The various Schmidt numbers considered were, 10, 50, 100, 150 and 200. The variation in the Schmidt number is expected to greatly influence the corrosion/precipitation rate since it is inversely

proportional to the diffusivity. The study has been carried out for both the laminar and turbulent regimes. The other properties of the fluid for the analysis were kept constant and same as the benchmark study runs.

Figure 35, shows the plot of variation of concentration flux with the non-dimensional loop length for laminar flow and figure 36 shows the same plot for the turbulent flow. It can be observed from both the figures that, higher the Schmidt number is higher is the corrosion rate and lower is the precipitation. The points of maximum corrosion and precipitation, of course, are not affected by the variation. Hence, for longevity of the life of the MTL, the Schmidt number should be kept as low as possible.

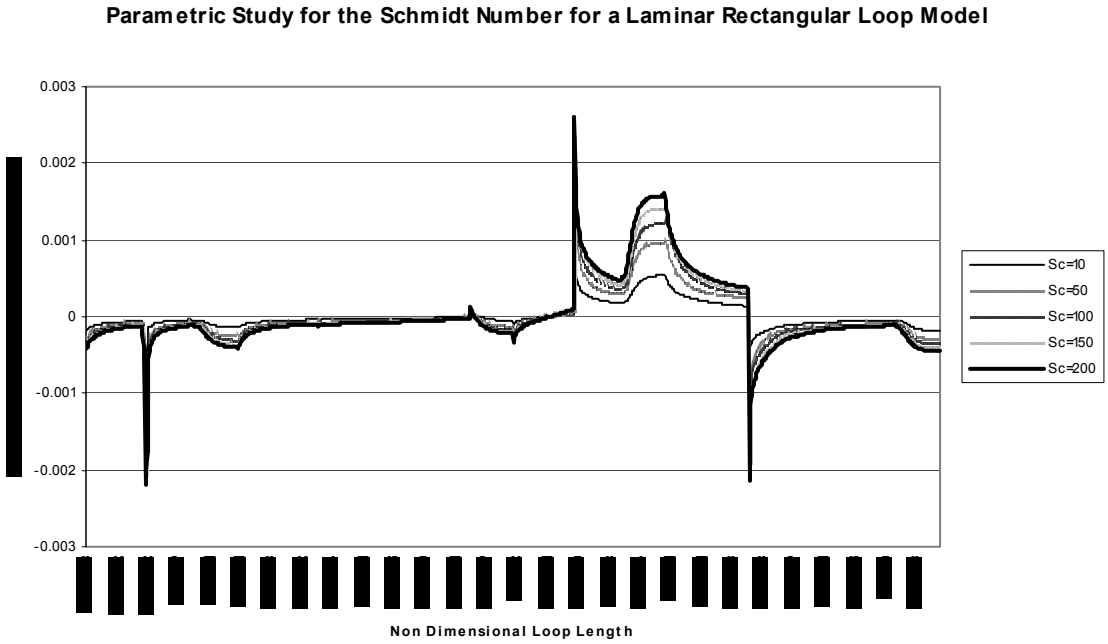

Figure – 35: Parametric study in Schmidt number for laminar rectangular loop model

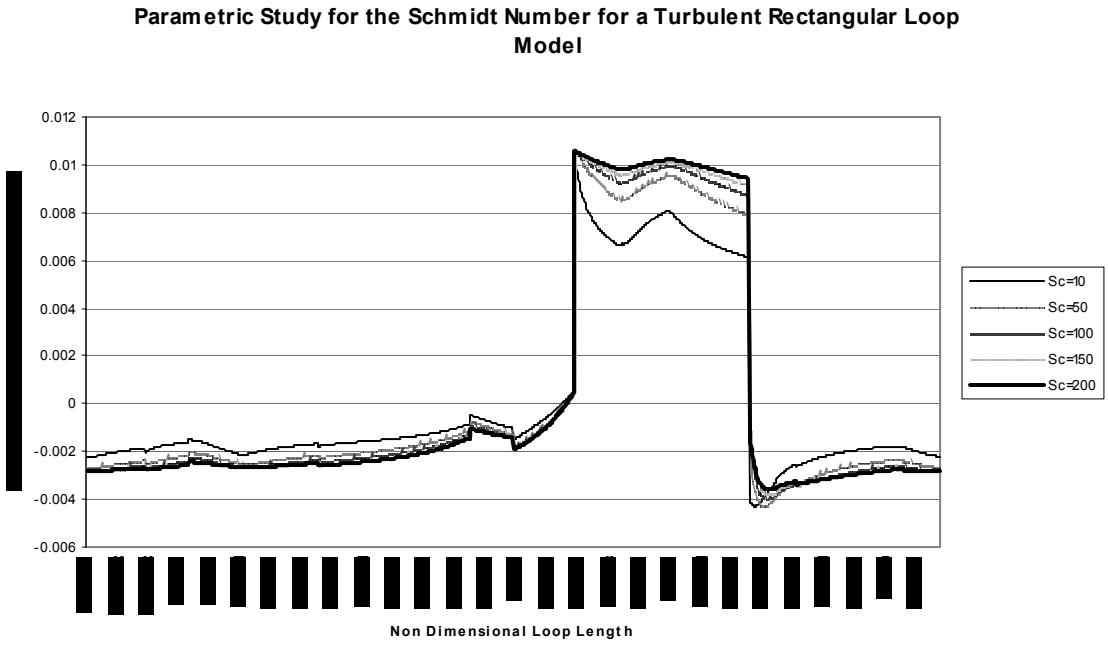

Figure – 36: Parametric study in Schmidt number for a turbulent rectangular loop model

Initial Oxygen Concentration:

The concentration of wall, as described before, is a function of initial oxygen concentration and temperature. The corrosion/precipitation rate is directly proportional to the wall concentration.

Four different initial oxygen concentrations have been considered for the study. The simulations have been run both in the laminar and turbulent regimes. The initial oxygen concentrations that have been considered are 0, 0.0001, 0.001 and 0.1. Figures 37 & 38 show the variation of concentration flux with the variation of initial oxygen concentration for the laminar and turbulent regimes respectively. It can be clearly visualized that the initial oxygen concentration highly affects the overall corrosion/precipitation rate. Higher the oxygen concentration is, higher is the corrosion/precipitation rate.

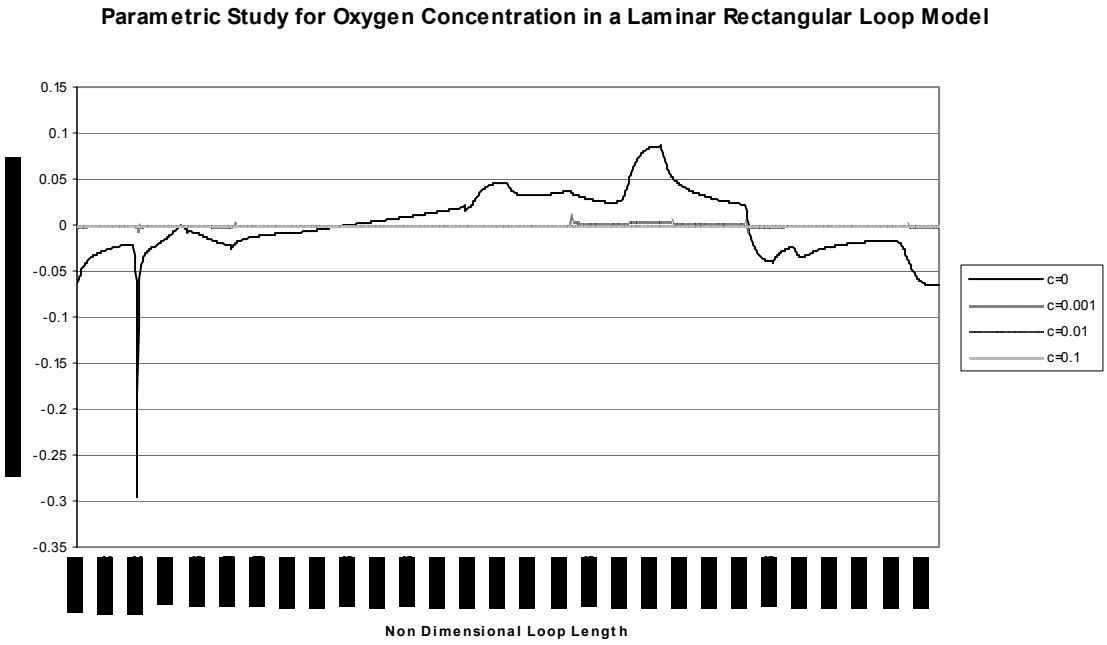

Figure – 37: Parametric Study in Initial Oxygen Concentration for Laminar Flow

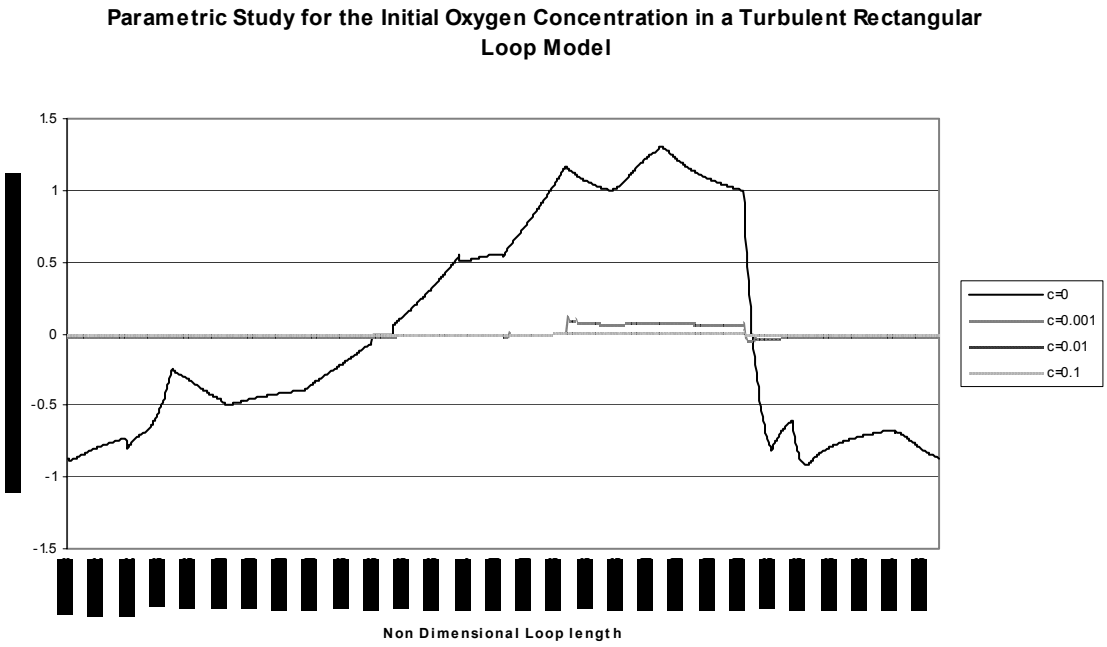

Figure – 38: Parametric Study in Initial Oxygen Concentration for Turbulent Flow

The case where the initial oxygen concentration is zero has been analyzed for comparison purposes. It can be seen that introduction of oxygen greatly reduces the corrosion of the steel surfaces.

Temperature Variation across the Loop Length:

The final parameter considered for the parametric study is the wall temperature variation along the loop length. Hence, by varying the wall temperature along the loop length has a direct affect on the wall concentration, which in turn affects the corrosion or precipitation rate. For the benchmark study, the temperature gradient considered was 200^{o}C i.e. 623K – 823K. Five different temperature differences have been considered for doing the parametric study. The temperature gradients considered were, 50K, 100K, 150K, 200K and 250K. For all the five cases, the base temperature has been maintained at 623K. The imposed wall temperature trend along the loop length is also similar to the figure 39 for all the cases. The remaining parameters have been kept at the original conditions for the analysis. Simulations have been carried out in both laminar and turbulent regimes. Figures 40 & 41 show the plot of corrosion/precipitation rate vs. the Loop length for various temperature ranges along the loop length for the laminar and turbulent regimes respectively.

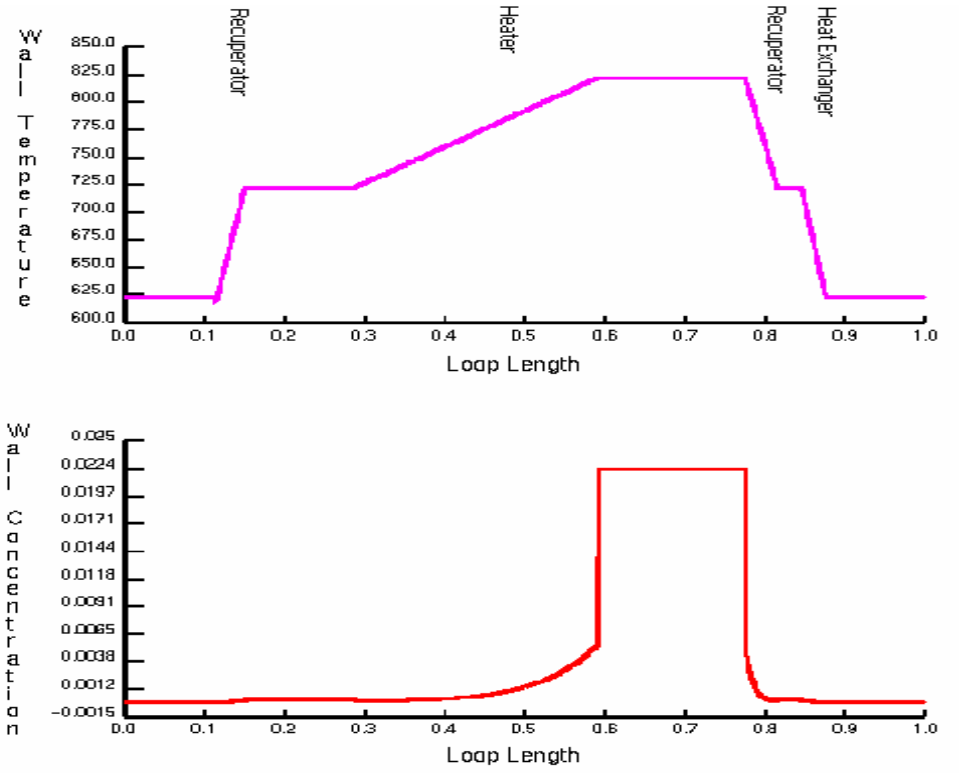

Figure – 39: Imposed wall temperature and concentration for the MTL

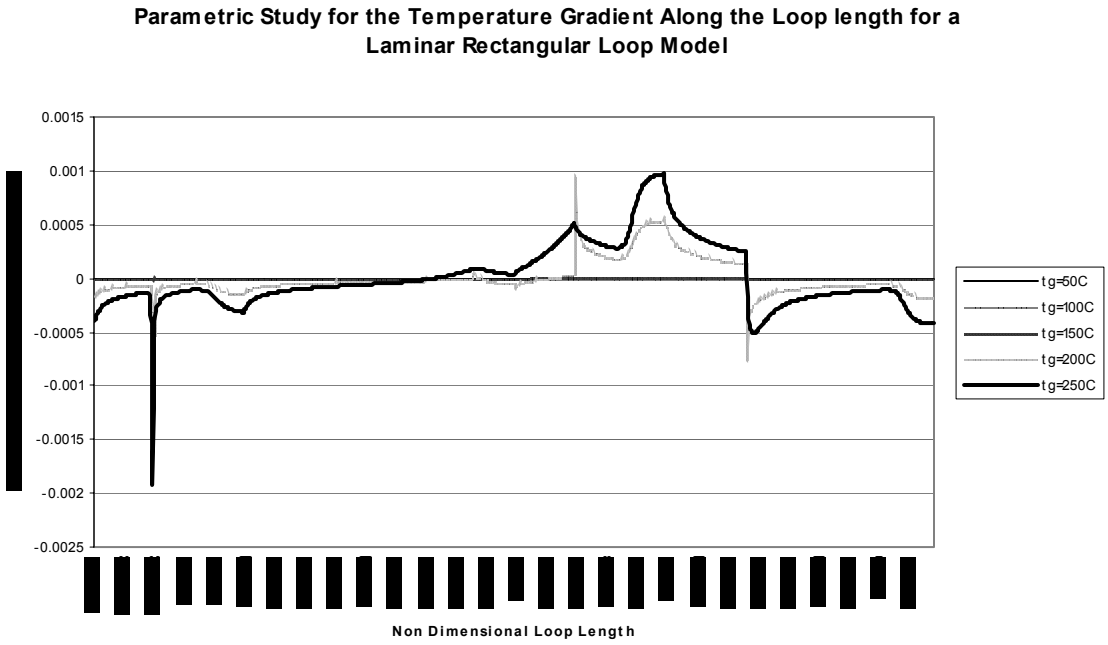

Figure – 40: Parametric study of the Temperature variation along the Loop Length for a Laminar Regime

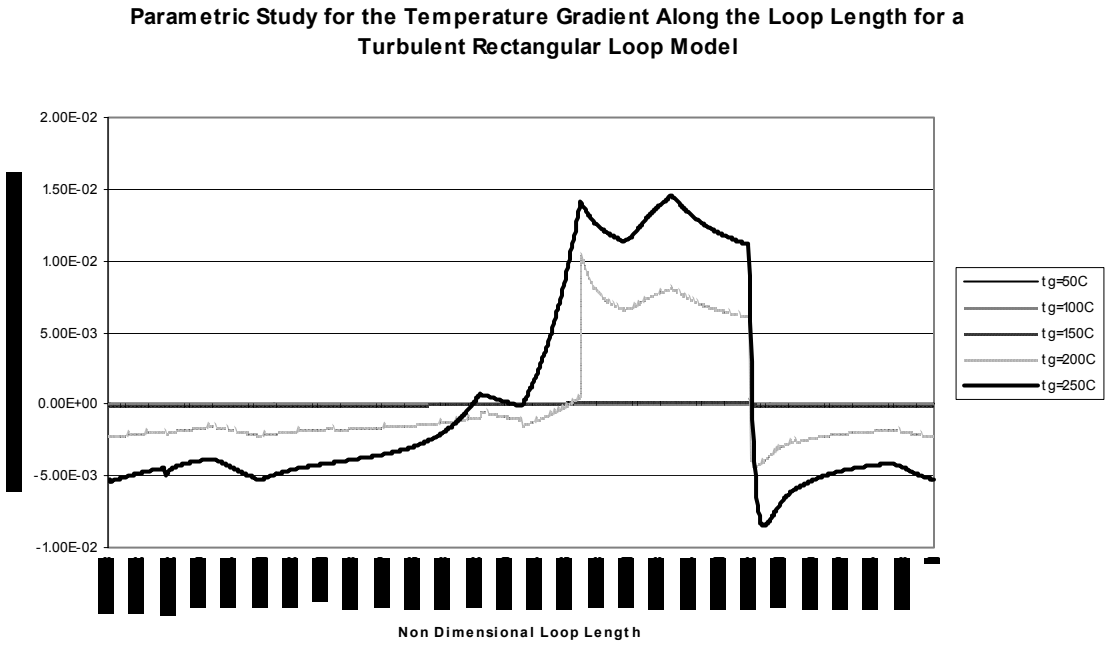

Figure – 41: Parametric study of the Temperature variation along the Loop Length for a Turbulent Regime

It can be deduced from the figures that the corrosion rate increases with the increase in the temperature gradient. The effect of temperature on the corrosion is very high. A 50K increase in the temperature highly increases the corrosion/precipitation rate as is obvious

from the figure. Hence the temperature gradient should be kept at minimum possible levels for the long run of the loop.

Local Corrosion Modeling:

Benchmark

Benchmark is important in research, especially in numerical simulation. It provides the validation of the tools and the base for the further effort. Before used to carry out calculation for more complicated cases, the code was applied to a classic problem and compare outcome with widely accepted results. Incompressible flow in sudden expansions is one of the classical problems and suits our calculation domain perfectly.

In this chapter, a model of sudden expansion is created. The diameter at the inlet was selected as 0.0254m. The lengths of the inlet and outlet regions are taken as 10 diameters. The ratio of the inlet to outlet diameter is 1:2. The total number of the cells in the model is 225,000. The aspect ratio considered is less than 10 as specified by the CFD package. Dry runs were simulated for the Reynolds number of 100 and 150. The simulated results obtained are as shown.

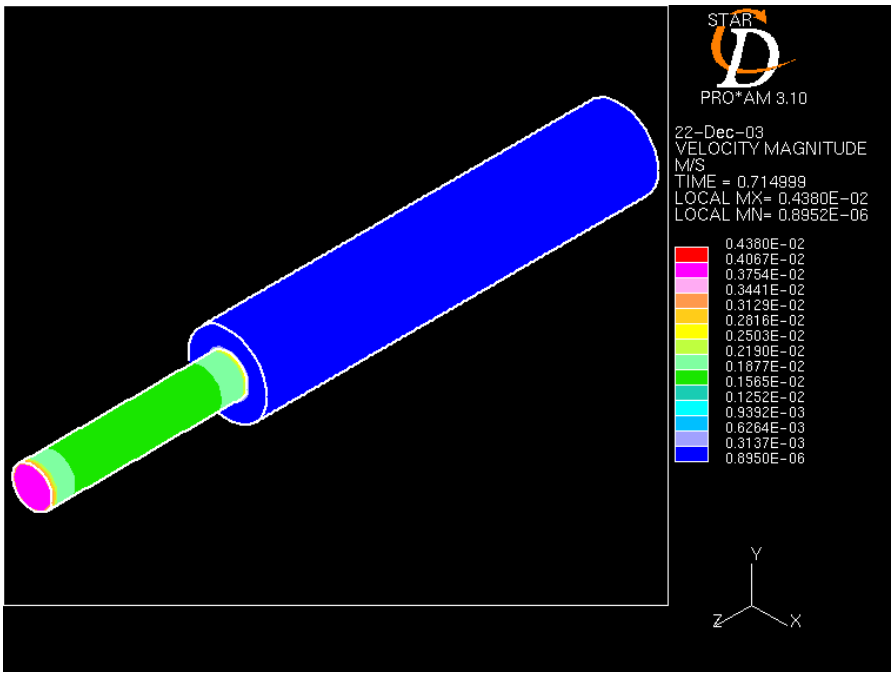

Figure – 41: Velocity profile for Reynolds number of 100

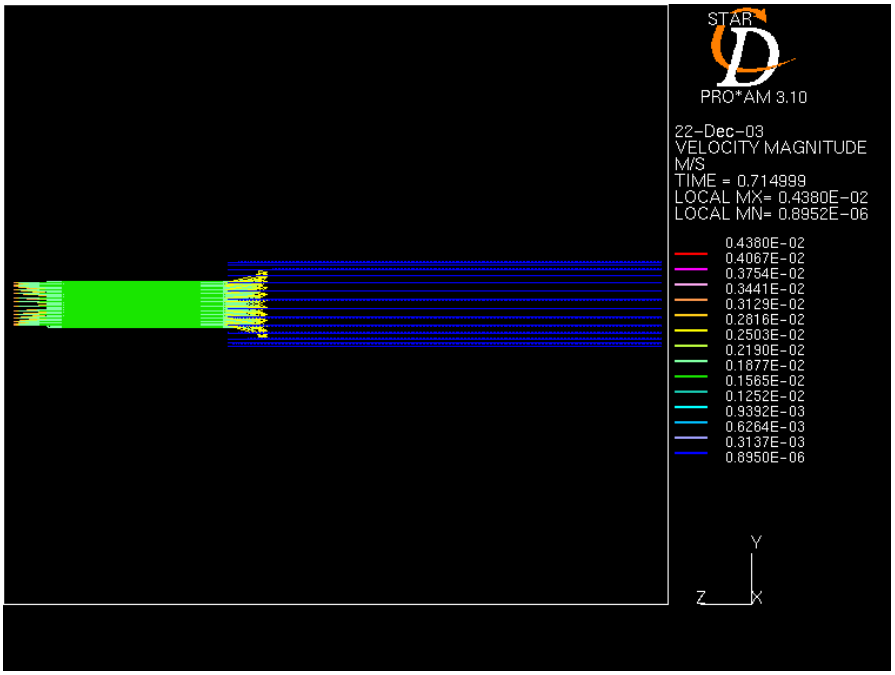

Figure – 43: Velocity vectors for Reynolds number of 100

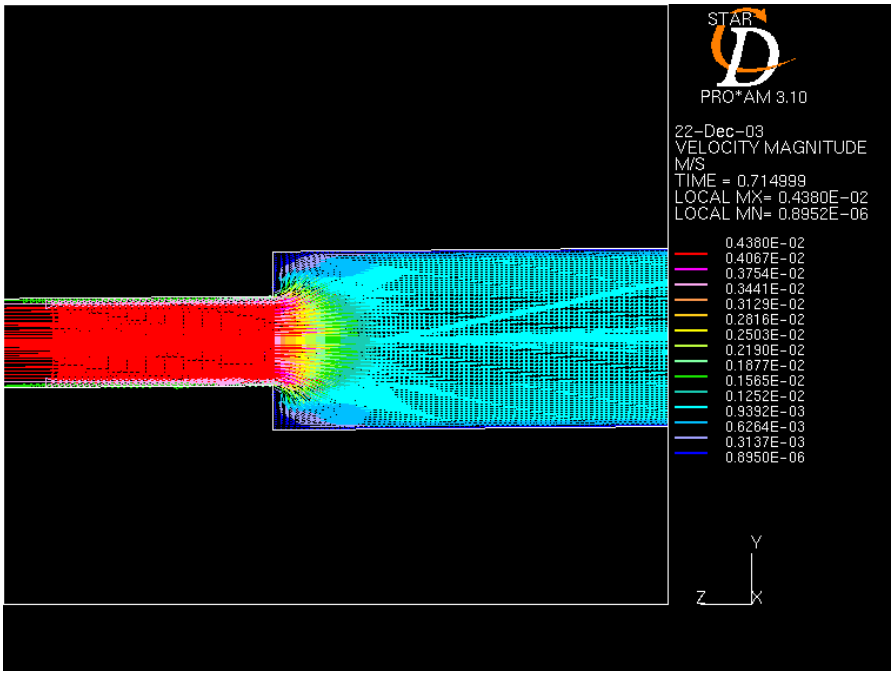

Figure – 44: Velocity magnitude for Reynolds number of 100 at the expansion section

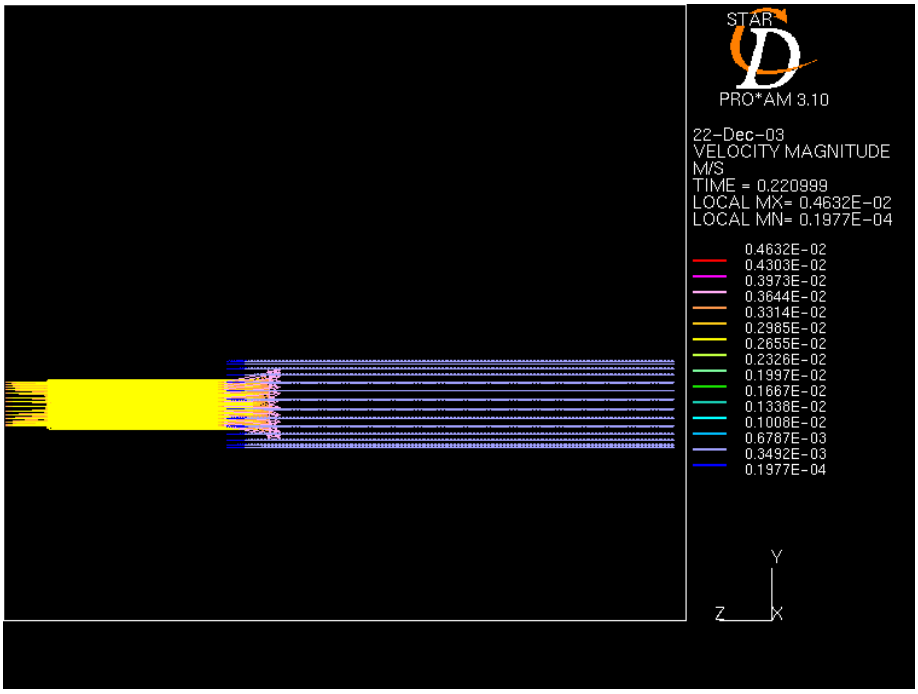

Figure – 45:Velocity vectors for a Reynolds number of 150

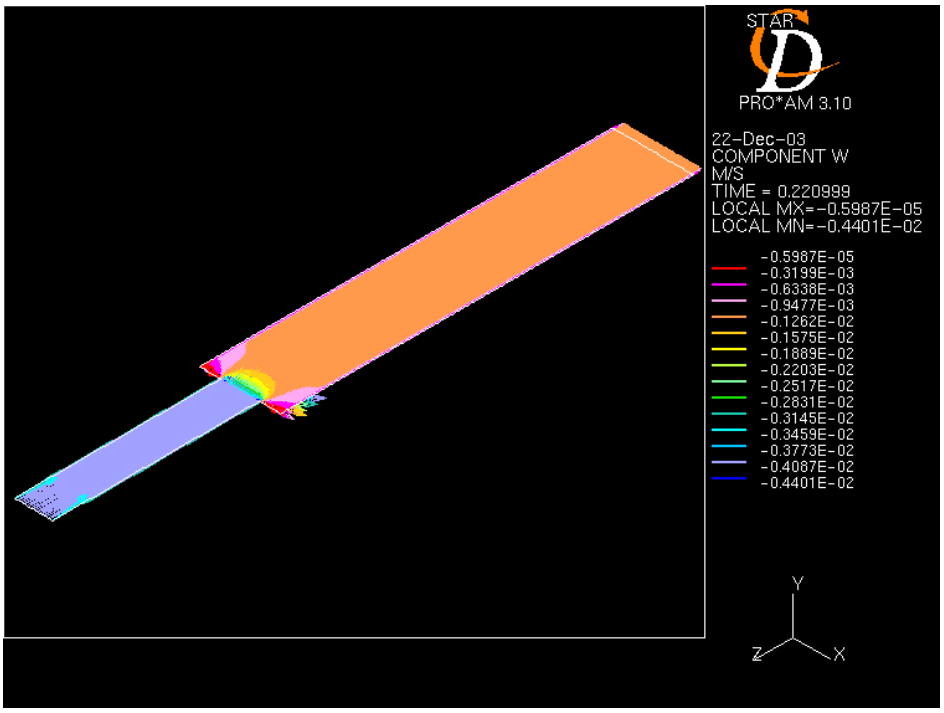

Figure – 46:Velocity component for a Reynolds number of 150